Hochschule Karlsruhe
Technik und Wirtschaft
UNIVERSITY OF APPLIED SCIENCES

Analysis and measurements of thermally induced processes in insulated plastic pipes

- English version -

CONFIDENTIAL

Bachelorarbeit (B.Eng.)
Nr. 18/049

Von
Timo Klumpp
geb. am 08.10.1993
in Calw

Betreuer der Fa. Georg Fischer Piping Systems GmbH:
Dipl. Ing. Hanspeter Müller

Betreuer der Hochschule Karlsruhe:
Prof. Dr.-Ing. h. Michael Kauffeld
Dipl. Ing. (FH) Timo Maurath

Karlsruhe, Thursday, 04 October 2018

Note of thanks

At this point, I would like to thank all participants who contributed to the success of this work through their professional or personal support.

First of all, I would like to thank my supervising professor, Prof.Dr.-Ing. habil. Michael Kaufffeld, for his support and evaluation of my work.

Likewise my thanks Dipl.-Ing. (FH) Timo Maurath, who contribute significantly due his patience, interest, helpfulness, suggestions and discussions during the implementation.

A very special thanks goes to the company Georg Fischer, especially Dipl.-Ing. Hanspeter Müller for his professional support, as well as all participants of the numerous telephone conferences, for the provision of the topic. The wellbeing in the cooperation was always present, so I won´t fail to me say thanks at this point for the friendly cooperation and the trust in me.

Finally, I would like to thank my family, which has motivated me a lot. Also thanks to my girlfriend at this point.

Statutory declaration

I declare that I have authored this thesis independently, that I have not used other than the declared sources / resources, and that I have explicitly marked all material which has been quoted either literal-ly or by content from the used sources.

Ort, Datum Unterschrift

Kurzfassung (Deutsch)

Ziel dieser Arbeit war es, verschiedene Einbausituationen von Rohren der Fa. Georg Fischer Piping Systems, bei möglichst realitätsnaher Belastung zu untersuchen.
Hierzu wurden zunächst mehrschichtige Rohre, sowohl mit, als auch ohne Glasfaserverstärkung, einer freien Längenänderung, aufgrund einer Temperaturänderung zwischen -50 °C und +70 °C, unterzogen. Die Ergebnisse hierbei zeigen die Abnahme der längenbezogenen Ausdehnung mit zunehmendem Glasfaseranteil, was auf eine längsseitige Ausrichtung der Glasfasern schließen ließ. Die Ausdehnung bei Rohren mit 30 Gew.-% Glasfasern betrug lediglich noch knapp ein Viertel von der des Referenzrohres.

In zweitem Versuch wurden die Axialkraftmessungen des Vorgängers vergleichend an CF 4.0 Rohren der gleichen Dimension durchgeführt. Die Ergebnisse zeigen, dass, aufgrund des größer werdenden Durchmesserverhältnisses, auch die Kräfte in fest eingespanntem Zustand zunehmen. Hierbei war die maximale Zugkraft von acht Kilonewton, aufgrund zunehmendem E-Modul für kalte Temperaturen, leider nicht mehr ausreichend, alle Rohre bei -10 °C und -30 °C auf Referenzlänge zurück zu stellen. Beim Vergleich mit den Ergebnissen der Vorgängermessung konnte festgestellt werden, dass die Differenz der resultierenden Kraft, zwischen CF 2.0 und CF 4.0, mit tiefer werdender Temperatur zunimmt.

Neben der Axialkraft wurden auch die Messungen am Biegeschenkelprüfstand vergleichend an CF 4.0 Rohren durchgeführt. Die Ergebnisse hierbei zeigen in der thermisch bedingten Kraft große Übereinstimmungen. Die überzogene Auslängung zeigt hierbei keine Tendenz und muss in weiteren Messungen verifiziert werden. Der Ausfall der Pumpe zwang zum vorzeitigen Abbruch des Versuches.

Ein weiterer Versuch beschäftigte sich mit dem zeit- und temperaturabhängigen Durchbiegeverhalten verschiedener Rohrleitungen. Hierzu wurde ein Versuchsstand konstruiert, der es ermöglicht, das zeitabhängige Durchbiegeverhalten messtechnisch zu erfassen, um resultierende Steifigkeitsgrößen ableiten zu können. Für den Versuch kamen, neben verschiedenen Einfachrohren, unter anderem CoolFit Rohre mit und ohne mittig angeschweißtem Fitting, sowie die mehrschichtigen glasfaserverstärkten Rohre aus dem Ausdehnungsversuch, zum Einsatz. Bei Betrachtung der Ergebnisse von Einfachrohren kann die Abnahme des E-Moduls mit zunehmender Temperatur erkannt werden. Außerdem kann bei Rohren aus PP-H eine maximale Änderung des E-Moduls zwischen kalten und warmen Temperaturen, während bei Rohren aus PB-H kaum eine Änderung des E-Moduls in bestimmten Temperaturbereichen beobachtet wird. Die Betrachtung mancher Ergebnisse ließ eine Ergebnisstreuung vermuten, was sich in Reproduzierbarkeitsversuchen auch bestätigt hat.
Die CoolFit Rohre ergaben in ihrem Durchbiegeverhalten die gleichen E-Module wie die entsprechenden Einfachrohre, allerdings unterschieden sie sich in ihrem Kriechverhalten. Die mittigen Fittings stellten sich dabei als Schwachstelle heraus. Anders die Schweißverbindung von ecoFit Rohren, hierbei war zwischen durchgehendem und geschweißtem Rohr kaum ein Unterschied festzustellen. Das glasfaserverstärkte Rohr ergab, wie erwartet, größere E-Module. Bei einer abschließenden Bewertung des Kriechverhaltens konnten Temperaturbereiche mit gleichem Verhalten, tendenzielle Abnahmen und eine zunehmende Kriechbeständigkeit mit zunehmender Temperatur festgestellt werden.

Ein abschließender Versuch sollte den Einfluss von Solarstrahlung auf den Verzug von im freien gelagerten, als auch fest verbauten Rohren simulieren. Hierzu wurden in Vorversuchen die verschiedenen Parameter für die Simulation untersucht und dann an einem Prüfstand für die Versuchsdurchführung eingestellt. Eine Kundenangabe gab vor, dass die Oberflächentemperatur zu +60 °C eingestellt werden sollte. Diese konnte für die Versuche gut und gleichmäßig eingestellt werden. Bei Betrachtung der Ergebnisse konnte festgestellt werden, dass die frei gelagerten Rohre bei dieser Temperatur einen maximalen Verzug von ungefähr einem Zentimeter aufweisen. In der eingebauten Situation konnte kein wirklich messbarer Verzug festgestellt werden. Nach Abkühlen der Rohre kehrten sie wieder in ihre Ausgangsform zurück.

Abstract (English)

The aim of this work was to investigate different Georg Fischer pipe installations with a lifelike load. Therefore, there were multi-coated pipes with different glass fibre contents, which were subjected to a free change in length because of the temperature in a range between -50 °C and +70 °C. The results showed the decrease of length related expansion by increasing glass fibre content, which suggests a longitudinal orientation. The expansion of pipes with 30 wt.-\% was only a quarter compared to the reference pipe.

The second test repeated the axial force predecessor measurements comparative with CF 4.0 pipes by the same inner diameter. The results showed that due to the increasing diameter ratio, the forces in firmly clamped state increase also. Unfortunately, the maximum tensile force of eight kilo Newton was no longer sufficient to reset all pipes to their reference length at -10 °C and -30 °C. The comparison with the previous measurements showed that the difference of the resulting force between CF 2.0 and CF 4.0 increases by decreasing temperatures.

Next to the axial force, there was the L-Bent build-up measurements, which was comparatively done for the CF 4.0 pipe systems. The results shows accordance in the thermal force. The coated extension shows no tendencies and has to be verified in further measurements. The failure of the pump forced to stop the experiments prematurely.

Another attempt investigated the time dependent deflection behaviour of various pipelines. For this purpose a test stand was designed, which makes it possible to measure the time dependent deflection behaviour by measurement. This made it possible to derive resulting strength parameters. In addition to various single pipes, there were also CoolFit and multi coated pipes. Both are checked with and without central welded fittings. By considering the results of single pipes, the behaviour of the modulus of elasticity could be recognized well. By increased temperatures, the modulus decreased. There were pipes such as PP-H with a maximum range of their modulus of elasticity between cold and warm temperatures. Hardly any changes were detected in certain temperature ranges for pipes such as PB-H. The consideration of some results suggested a distribution of conclusions, which was confirmed in reproducibility experiments.
The CoolFit pipes yielded the same modulus of elasticity as the corresponding single pipes but they were different in their creep behaviour. The central welded fitting turned out to be a weak spot. Hardly any difference could be detected between welded and continuous ecoFit pipe. As expected, the fiberglass reinforced pipe resulted in larger modulus of elasticity. The creep behaviour of the single pipes showed temperature ranges with the same behaviour, tendency declines and even increasing creep resistance with increasing temperatures in a final evaluation.

A final trial stimulate the influence of solar impact on the distortion. For this purpose, the various parameters for the simulation were investigated in preliminary experiments and then set on a test rig for the experimental procedure. A customer specified that the surface temperature should be set to +60 °C. This could be adjusted well and evenly for the experiments. Looking at the results, it could be determined that the freestanding pipes have a maximum draft of about one centimetre at this temperature. In the installed situation, no measurable arrears could be determined. After cooling down all pipes, they returned to their original shape.

Table of contents

List of Figures

List of Tables

Nomenclature

Latin formula

Symbol	Unit	Definition
A	mm^2	Area
$\dot{Q}$	W	Heat flow
$\dot{q}$	W/m^2	Specific heat flow (in special cases also W/m)
d	mm	Outer diameter from flowed pipes
D	mm	Outer diameter from casing pipes
E	N/mm^2	Modulus of elasticity
F	N	Force
g	m/s^2	Gravitational constant
h	mm	Height
I	mm^4	Moment of inertia
l	mm	Length
m	kg	Mass
p	bar	Pressure
q	kg/m	Distributed load
R	m	Outer radius
r	m	Inner radius
s	mm	Depth
t	s	Time
T	°C	Temperature
wst	mm	Thickness
x	mm	Length at a various place
X	cm	Distance between radiation source and pipe surface
z	cm	Distance between two radiation sources

Greek formula

Symbol	Unit	Definition
α	1/K	Coefficient of thermal expansion
ΔL	mm/m	Thermal induced change of length per meter pipe
ϵ	mm	Deflection
λ	µm	Wavelength
λ_i	$W/(m \cdot K)$	Thermal conductivity
ξ	cm	Elastic line
ρ	kg/m^3	Density

Subscripts

Symbol	Definition
1	Reference to reference conditions (usually 20 °C)
1-2	Long lying pipe in L-bent buildup measurements
2	Measurement by new conditions
3	Measurement by new conditions
3-4	Deflection by L-bent buildup measurements
32A	Exit CF 4.0 d32
32E	Entrance CF 4.0 d32
32O1	Surface measurement CF 4.0 d32 number one
32O2	Surface measurement CF 4.0 d32 number two
63A	Exit CF 4.0 d63
63E	Entrance CF 4.0 d63
63O1	Surface measurement CF 4.0 d63 number one
63O2	Surface measurement CF 4.0 d63 number two
68	Depth of the PT-Element in the pipe
75	Depth of the PT-Element in the pipe
83	Depth of the PT-Element in the pipe
90°	Positioning at 90° around the scope
180°	Positioning at 180° around the scope
A	Outer
Ausl.	Deflection
Außenrohr	Reference to the outer pipe
B	L-Bent buildup
B32	Bow CF 4.0 d32
B63	Bow CF 4.0 d63
Bm.	Tape measure
Di.	Direct radiation
Gesamt	Summary
Gl.	Reference to the glass rod
i	General name
In	Indirect radiation
innen	Measure on the inner side
Innenrohr	Reference to the inner pipe
Isolation	Reference to the insulation
KK	Climate chamber
Links	Deflection of the L-Bent buildup to the left side
m	Average
max	Maximum
Messbereich	Reference to the measurement area
Symbol	**Definition**

Oberfläche	Reference to the surface
PE-außen	Reference to the outer surface of the PE
PE-innen	Reference to the inner surface of the PE
Prüfgewicht	Reference to the test weights
R	Provision
rechts	Deflection of the L-Bent buildup to the right side
R32	Surface pipe CF 4.0 d32
R63	Surface pipe CF 4.0 d63
Ref	Reference to reference pipe PE-100
Referenz	Reference
Th.	Thermally
Über	Crossing between insulation an inner pipe
Umg.	Referenc to environment
V-B	Connection to L-Bent
V32	Connection place CF 4.0 d32
V63	Connection place CF 4.0 d63
V3a	Reference to layer structure of V3a pipes
V3b	Reference to layer structure of V3b pipes
V5	Reference to layer structure of V5 pipes
V6	Reference to layer structure of V6 pipes
w	Real length
Z	Center

Topscripts

Symbol	**Definition**
*	Reference of the formula to a black radiator

1 Georg Fischer AG

1.1 The Georg Fischer Group

The Georg Fischer Group has been founded in 1802 as an industrial company and operates currently 136 companionships in 34 countries, by headquarters in Switzerland. In 2017, the approximately 16.000 employees could generate sales of CHF 4.150 million.

The group of companies includes three divisions: +GF+ Piping Systems, +GF+ Automotive and GF+ Machine Solutions.

+GF+ Piping Systems deals with piping systems made of plastic and metal for the safe transport of gas, water and chemicals. The product offering covers all the components of gas, water and chemical transport. +GF+ Piping Systems is represented in more than 100 countries and therein in the supply, the industrial and building service sectors. In addition, the division operates several research and development centres, as well as around 30 production sites in Europe, Asia, North and South America. In 2017 +GF+ Piping Systems generate sales of CHF 1.678 million.

+GF+ Automotive deals with cast solutions and systems made of aluminium, magnesium and iron for the global automotive industry and industrial applications. In addition, the division is still dealing with the CO_2 reduction of modern automobiles, through highly complex lightweight solutions. +GF+ Automotive produces in 13 locations. The research and development centres are located in Schaffhausen (Switzerland) and Suzhou (China). Sales by +GF+ Automotive in 2017 amounted CHF 1.482 million.

+GF+ Machine Solution deals with tool- and mold making parts as well as the production of precision parts. The division is represented in the aerospace, information and communications technology, medical technology and automotive industries. +GF+ Machine Solution has locations in more than 50 countries. In addition, the division operates research and development centres, as well as production facilities in Switzerland, Sweden, the USA and China. Sales could be generate in 2017 to CHF 992 million [1].

1.2 Vision and strategy

The vision is subdivided in:

- Safe transport of water and gas
- Safe vehicles and efficient energy consumption
- Precision manufacturing

The strategy is subdivided in:

- Expansion in growth markets
- Shifting the divisional portfolio into higher margin businesses
- Increase in sales and innovation strength

2 Structure and properties of the test pipes

2.1 Test pipes

There are different test pipes, which were used. The following chapters 2.1.1 until 2.1.4 will explain these in a short way.

2.1.1 Pipes without insulation

Pipes without an insulation will also be called as “naked pipes” by +GF+. The polymers of the pipes are explained in chapter 2.2.
In the name, the wall thickness is indicated next to the outer diameter. The designation of the pipe in chapter 2.1.5 Figure 1 out of the polymer Acrylonitrile-butadiene-styrene sounds “ABS d32x2,9”. In general is this “Polymer outer diameter x wall thickness”.

2.1.2 CoolFit ABS

CoolFit pipes, called as “CF” in the following report, are insulated. There are three different CF pipes which are explained in the following chapters. They are almost identical in their design and differ only in their diameter ratio between outer and inner pipe, as well as in their connection technology.
The inner pipe from CF ABS is made out of the polymer Acrylonitrile-butadiene-styrene (ABS), Chapter 2.2.1. For a shorter heat loss through the environment, CF ABS is insulated with polyurethane foam, Chapter 2.2.2. The outer pipe is from the polymer HDPE, polyethylene high density, Chapter 2.2.3 and gets his black colour through blended carbon. This makes it more resistance against UV-radiation. In comparison to other Polymers (PVC-U, PE, PP, PVDF) ABS is not chemical resistance. Therefore, it is characterized by the high impact strength for deep temperatures. Furthermore, it has, in contrast to polyethylene, an adhesive connection technology. That´s the reason why it is used often in explosive area where welding isn´t possible.
The nomenclature is similar to pipes without insulation with the difference that instead of the wall thickness the outer diameter of the outer pipe is specified. The name for the pipe in chapter 2.1.5 Figure 2 is “CF ABS d32/D75”, also frequently indicated as “CF ABS d32”.

2.1.3 CoolFit 2.0

The inner pipe from CF 2.0 is PE-100. It has also an insulation to reduce heat losses to a minimum. The outer pipe is also from the polymer PE-100. CF 2.0 and 4.0 pipes have a welded connection technology that could be done automatically through a welding machine from +GF+.
CF 2.0 pipes were used for the transport of cold water in large residential and commercial buildings, as well as data centers and process cooling systems.
The nomenclature is the same used for CF ABS. The pipe in chapter 2.1.5 Figure 3 is indicated as “CF 2.0 d32/D75” or “CF 2.0 d32”.

2.1.4 CoolFit 4.0

CF 4.0 is the youngest product family. Figure 4 compares CF 2.0 and 4.0. While the inner pipes have the same diameter, the diameter of the outer pipe increases. The polymers are the same. Through the bigger diameter ratio, the heat loss is more reduced compared with CF 2.0.

2.1.5 Drawings

The following figures visualize chapter 2.1.1 until 2.1.4.

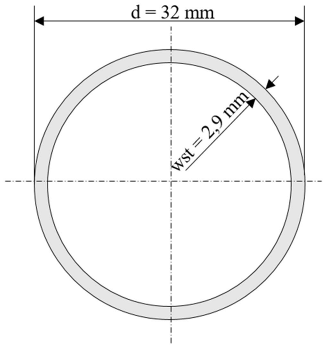

Figure 1: Schematic structure from Pipes without an insulation

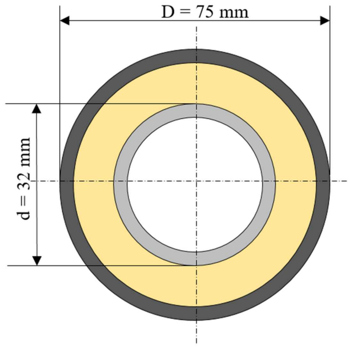

Figure 2: Schematic structure of CF ABS d32/D75

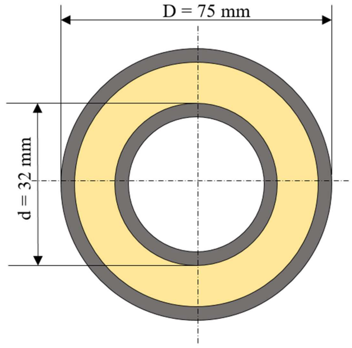

Figure 3: Schematic structure of CF 2.0d32/D75

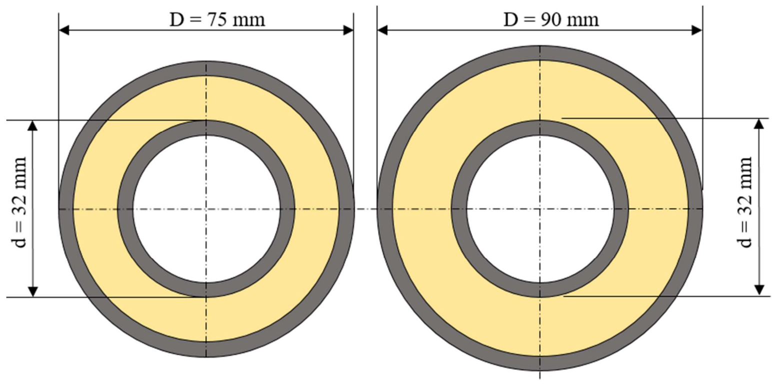

Figure 4: Comparison CF 2.0 and CF 4.0

2.2 Polymers

2.2.1 Acrylonitrile-butadiene-styrene

Acrylonitrile-butadiene-styrene (ABS), counts to the group of styrene polymers. In his structure, it belongs to amorphous thermoplastics. ABS counts, like Polyethylene, to the mass polymers. Due to its polarity and the associated adhesive joint is ABS often used where welding is not possible, for example in potentially explosive atmospheres. Next to pure ABS polymers, blends are also available. This allows setting properties depending on the mixing ratio of the plastics. Blends for ABS are Polyamide (PA-ABS), Polycarbonate (PC-ABS) or Polymethylmethacrylate (ABS-PMMA). Special characteristics are high impact strength, also in deep temperatures and a low thermal conductivity. [4, p. 120ff]
Table 1 shows more characteristics.

Table 1: Characteristics ABS [5]

Characteristic	Value	Unit
Density	1035	$kg \cdot m^3$
Yield stress at 23 °C	40	$N \cdot mm^{-2}$
Modulus of elasticity	1600	$N \cdot mm^{-2}$
Impact strength (Charpy) at 23 °C	42	$kJ \cdot m^{-2}$
Impact strength (Charpy) at -40 °C	10	$kJ \cdot m^{-2}$
Crystallite melt point	-	°C
Thermal conductivity at 23 °C	0,17	$W \cdot (m \cdot K)^{-1}$
Coefficient of thermal expansion	0,100	$mm \cdot (m \cdot K)^{-1}$
Water absorption at 23 °C	<= 45	%
Colour	9005 (graphite-black)	RAL

2.2.2 Polyurethane foam

Polyurethane foam is one of the cross linked polyurethanes. They are obtained from an addition polymerization as a step reaction. [6, p. 213]
There are hard foams that have mostly closed and soft foams that have closed and opened cells. Due his opened cells and the air trapped inside, the thermal insulation is high. That is the reason why he is used often in the automotive ore household industry therefore. [7, p.27]
The foam formation in PUR is caused by gas-forming or vaporizing additives during the mixing and cross linking with the reactant. Another possibility of foaming is the release of CO_2 during the reaction. [8, p. 532]

2.2.3 Polyethylene

Polyethylene counts to the group of polyolefin polymers. Due his market share of 30 %, he is like ABS also a mass polymer. That is also the reason why he is that cheap. Another subdivision classifies polyethylene into the group of semi crystalline and nonpolar thermoplastics. Depending on the polymerization the molecular weight, the molecular distribution, the average chain length and the degree of branching can be determined. Depending on these characteristics, the four main types of polyethylene results: [9, p. 85]

- Polyethylene high density, PE-HD
- Polyethylene medium density, PE-MD
- Polyethylene low density, PE-LD
- Polyethylene linear low density, PE-LLD

In general, the properties of polyethylene depend on their main type. In addition to the microstructure and the resulting density, they differ mainly in their strength values, such as the yield stress or the elasticity modulus. Polyolefin polymers are characterized by their good chemical resistance and good electrical insulation properties. [4, p. 89f]

Other names are used for pipes out of polyethylene. These are based on the creep rupture strength (MRS) at 20 °C after 50 years with the test medium water. Table 2 shows the observed values, which according to DIN. [10, p.7]

Table 2: MRS from PE-80 and PE-100

Test pipe	**MRS in MPa**
PE-80	8,0
PE-100	10,0

The pipes by GF+ are out of PE-100 and get his black colour through the additive carbon. The reason is to make them more resistance against UV-radiation of the atmosphere. Table 3 shows some technical data by Georg Fischer of PE-100.

Table 3: Characteristics of PE-100 [5]

Characteristic	**Value**	**Unit**
Density	950	$kg \cdot m^3$
Yield stress at 23 °C	25	$N \cdot mm^{-2}$
Modulus of elasticity	900	$N \cdot mm^{-2}$
Impact strength (Charpy) at 23 °C	83	$kJ \cdot m^{-2}$
Impact strength (Charpy) at -40 °C	13	$kJ \cdot m^{-2}$
Crystallite melt point	130	°C
Thermal conductivity at 23 °C	0,38	$W \cdot (m \cdot K)^{-1}$

2.2.4 Other polymers

Chapter 2.2.1 until 2.2.3 describes the main polymers from this report. But there are also other polymers used in some tests which will be explained in the following numbering.

1. **Polyvinylchloride:**
   Polyvinylchloride (PVC), is one of the bulk plastics, like PE, and comes in third with a consumption of 32 million t/a. Due its additives, it has the widest range of applications. These make it possible to produce very powerful compounds. For the experiments, PVC-C and PVC-U are used.
   PVC-C has adjustable flexibility, good electrical properties in the low-voltage and low frequency ranges and a high chemical resistance.
   PVC-U, on the other hand, is characterized by the high mechanical strength, stiffness and hardness, impact sensitivity when unmodified in cold conditions, transparency in unfilled state, good electrical properties in low frequency ranges, high resistance to chemical attack and self-extinguishing after removing the ignition source. [11, p. 293]

2. **Polypropylene:**
   Polypropylene (PP) lies with a market share of 45 million t/a behind polyethylene on the second place of bulk polymers. The main applications are, due his food authenticity, in the food packaging and fiber area. Next to these main applications, PP will be used more and more in the automotive and consumer section. [11, p. 213]
   Isotactic, high heat resistance polypropylene will be used in the tests (PP-H). Excellent sliding properties, extreme wear resistance, high impact resistance and very good durability against chemicals characterize the materials of this product family. [12]

3. **Polybutene:**
   Polybutene (PB) is available in four different crystal forms, which can be formed from the melt during crystallization and can be converted during processing or time. Due his density of 0,91 g/cm³, Polybutene is a light material. His properties can be compared with PE-LD. It´s characterized by the high dimensional stability in the heat, high flexibility, even in the cold, low embrittlement temperature, high toughness, high abrasion resistance and high chemical resistance. [11, p. 254f]. For the experiments, PB-H is used.

4. **Polyvinylidenefluoride:**
   Polyvinylidenefluoride (PVDF) is a high molecular homopolymer. It`s structure depends on the production process. For example the degree of crystallinity depends very much on the thermal history of the mouldings. Quick cooling of the non-shaped mouldings and foils leads to transparent products, slow cooling or post-hardening leads too highly crystalline products of higher rigidity and pressure stability. PVDF is characterized by the following properties. It has a high mechanical strength, rigidity and toughness, a relatively high temperature resistance at low temperatures and a high chemical resistance. [11, p. 587]

3 Preliminary work

The work is based on the results of a previous thesis. Due to further tests with new pipes at the existing test labs, they will be explained in their design and function in the following chapters. There is, on the one hand, the axial force test lab, Chapter 3.1 and on the other hand the L-bent buildup, Chapter 3.2.

3.1 Axial force test stand

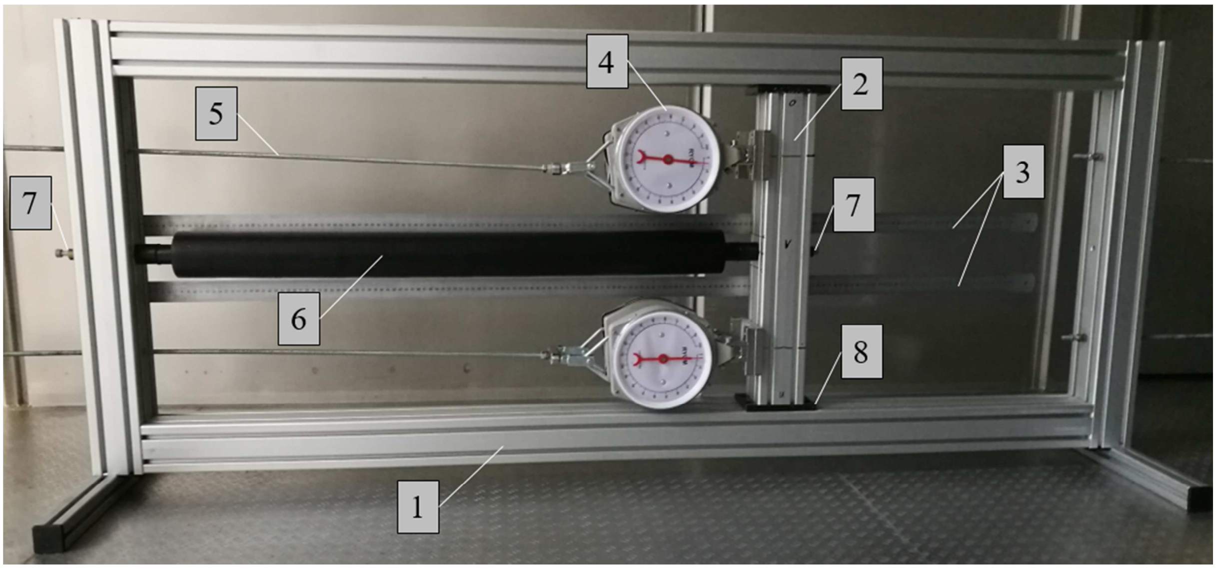

Figure 5: Design of the axial force test stand and numbering of his components

The axial force test stand exists of a frame construction {1}, an vertical sliding beam {2}, two parallel mounted steel rulers {3}, four analog scales {4} and two threaded rots {5}. Between frame and vertical slide beam is the testing pipe {6}, which is fixed with the frame construction on the left side and the vertical slide beam on right side through smaller threaded rots {7} in the inner pipe.
At the beginning of each test, the length of the test pipe at reference temperature of 20 °C will be measured by both steel rulers. This average length is used as reference. With this measure, a possible imbalance of the vertical slide bar can be counteracted. After that, the target temperature is set. The pipe changes its length and gets longer for warmer resp. shorter for colder temperatures. To accommodate this movement, the vertical slide beam is fixed by sliding rails {8} with the frame construction and can change his axial position without a force impact. After reaching the target temperature, the changed length will be measured and the analog scales will be mounted. After that, the threated rots produce an axial force, which is showed on the analog scales, and pulling the test pipe back to his reference length. It is important to note, that every material change his length due to changing temperatures. That is the reason, why the real length of the steel rulers has to be calculated via the thermal expansion coefficient first. That applies for both, the increase of length as well as the decrease of pipe length.
After measuring all data, the same procedure is being repeated after one, two and three hours. The results of the measured data´s are the declines of the axial force, while keeping the length of the test pipes for a reference temperature of 20 °C constant.
For a detailed description, please refer to the previous work. [13, p. 25ff]

3.2 L-Bent buildup

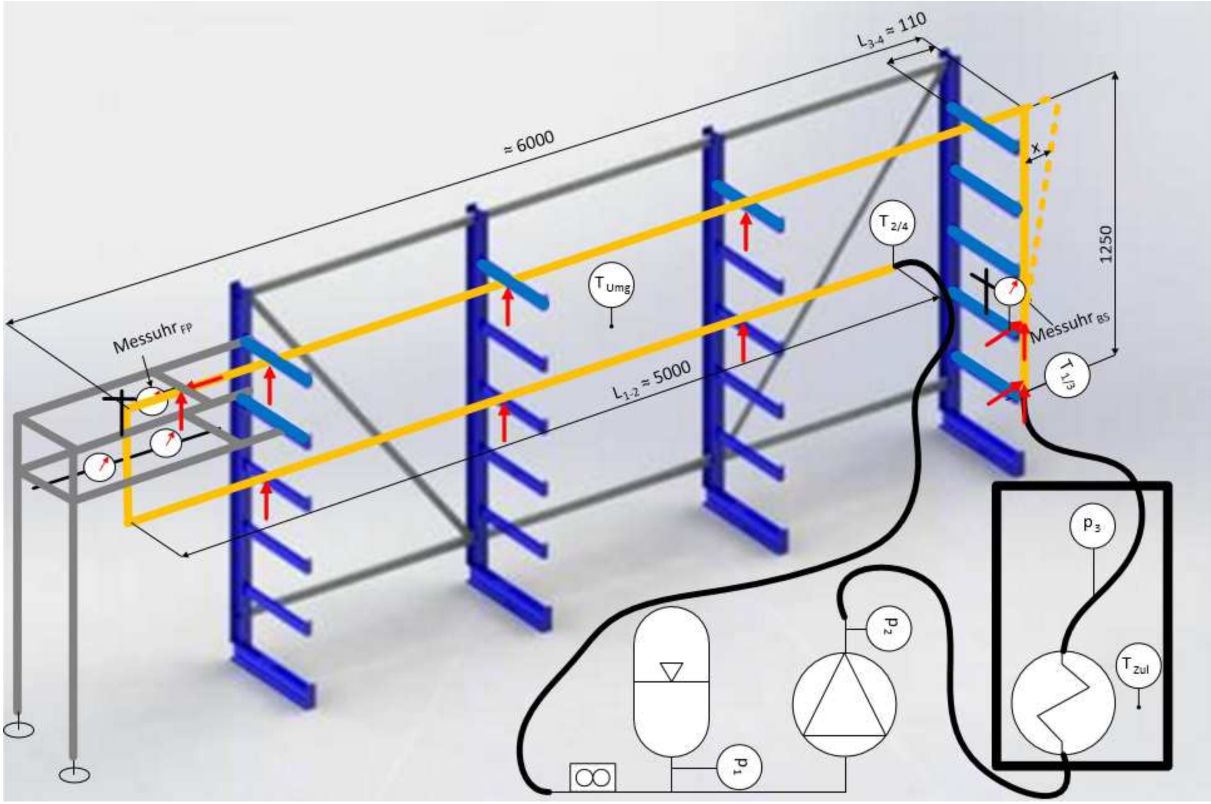

Figure 6: The construction of the L-Bent buildup for preliminary tests

The L-Bent buildup is a test construction to check the resulting forces for the installation variant bending leg. The preliminary tests check them for CF 2.0 d32/D75 and CF 2.0 d63/D110. Both pipes are connected in series. Figure 6 shows just one pipe to get a better overview and to describe the basic structure of the test lab.

The test buildup is located in the pipe rack next to the climatic chamber. He has on the right side, shown with a dashed line, the examined bending leg. This dashed line shows a standing pipe, which is hold at the bottom side by to fixing points. Due to the temperature of the medium flowing through it, the L-Bent buildup bends to the left side for colder and to the right side for warmer temperatures. The result is a bending line of the standing pipe (dashed line). A fix-point, which can be opened, holds the lying pipe on the left side. Thus the resulting force bends the vertical pipe. After bending and if no temperature changings could be detected anymore, the fixed point becomes opened and the bending will be fixed to a 90°-position. After that, the analog scales adjust the measured bending again and the force becomes noted. Furthermore, the lying pipes has clip it points in a too large dimension as guide rail to reduce the friction to a minimum.

Knowledge about the expansion behavior can be won by the lower pipe run. The medium flowing through is a propylene glycol / water mixture.

The hydraulic circuit provides a pump for conveying the fluid. The temperature can be adjusted to a desired temperature by a heat exchanger, which is located in the climate chamber, by their temperature control. A compensating vessel is switched in front of the pump for pressure monitoring. Have a look to the previous work for a detailed description. [13, p.41 ff.]

4 Axial force measurements

4.1 Test mode

The preliminary tests shell comparative done for CF 4.0 pipes of the dimension d32, d50 and d63. The test temperatures are the same. Table 4: Test temperatures for the axial force tests shows these.

Table 4: Test temperatures for the axial force tests

Name	Target temperature	ΔT to the reference temperature
T-Positive	+60 °C	+40 K
	+40 °C	+20 K
T-Reference	+20 °C	$\pm$0 K
T-Negative	-10 °C	-30 K
	-30 °C	-50 K

4.2 Test procedure

The experiment takes a lot of time and should be carried out at the same time as the measurements of the deflection (Section 7). Because of this, it is necessary to change the experimental procedure of the predecessor work accordingly. The following numbering shows the procedure:

1. Set the climate chamber to reference temperature of 20 °C
2. Measuring of the reference data´s
3. Calculation of the reference length while target temperature due to thermal expansion
4. Set the climate chamber to target temperature about the night
5. At 1pm of the following day, while the deflection measurements is going on since at least four hour: Starting of the axial force measurement through check of the length for target temperatures
6. Putting in the analog scales and set them to zero kilogram
7. Pulling the test pipe back to calculated reference length
8. Reading of the analog scale forces and note them in the protocol
9. Waiting for approximately one hour
10. Repeat point 7 until 9 three more times
11. Putting out the analog scales and relax the test pipe about night
12. Set the climate chamber to a new **target temperature** about night
13. Repeat point 5 until 11

The predecessor set the climate chamber about night to a temperature of 20 °C and could take the reference length again. The target temperature was set about the day and the procedure could be done in the evening. The procedure described in 1 until 13 has the difference that he set the new target temperature about night. Because of this, it is no longer possible to see the influence of a permanent compression or extension of the pipes.

4.3 Results

4.3.1 Overview of the results

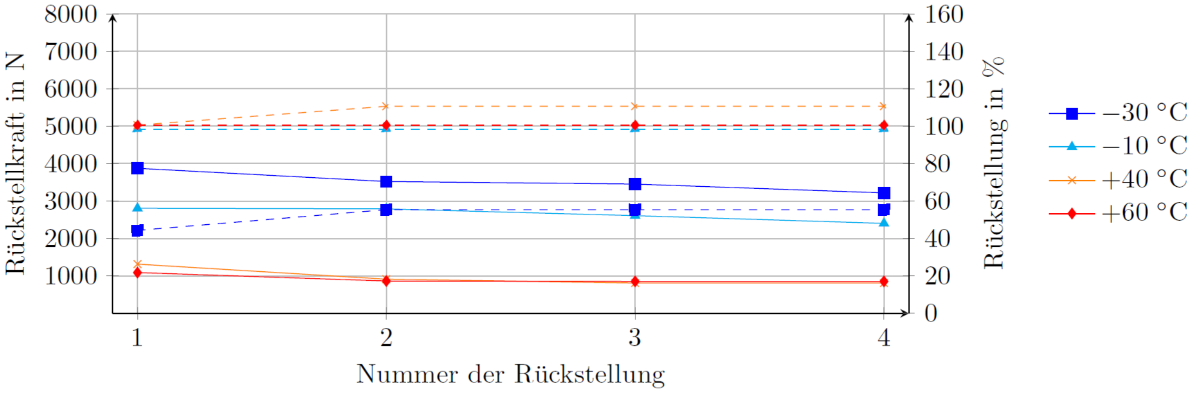

Figure 7: Results axial force measurements CF 4.0 d32/D75

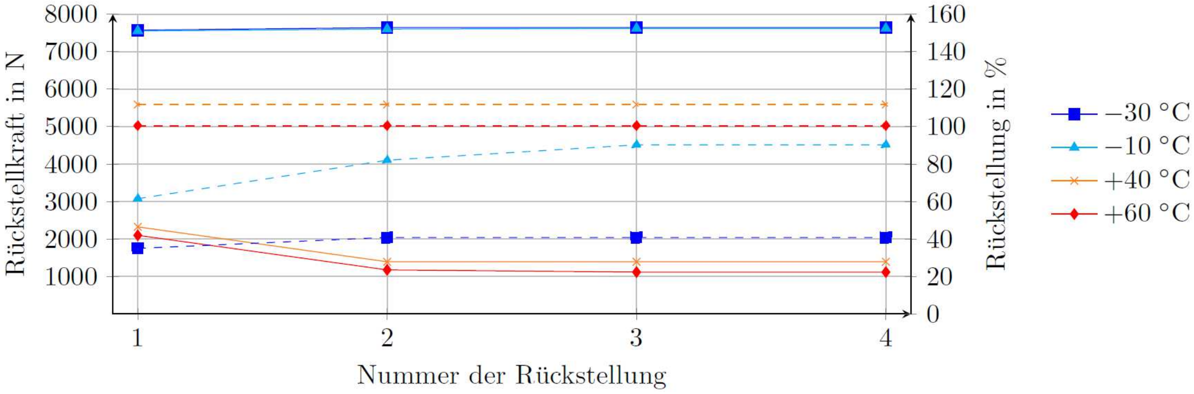

Figure 8: Results axial force measurements CF 4.0 d50/D110

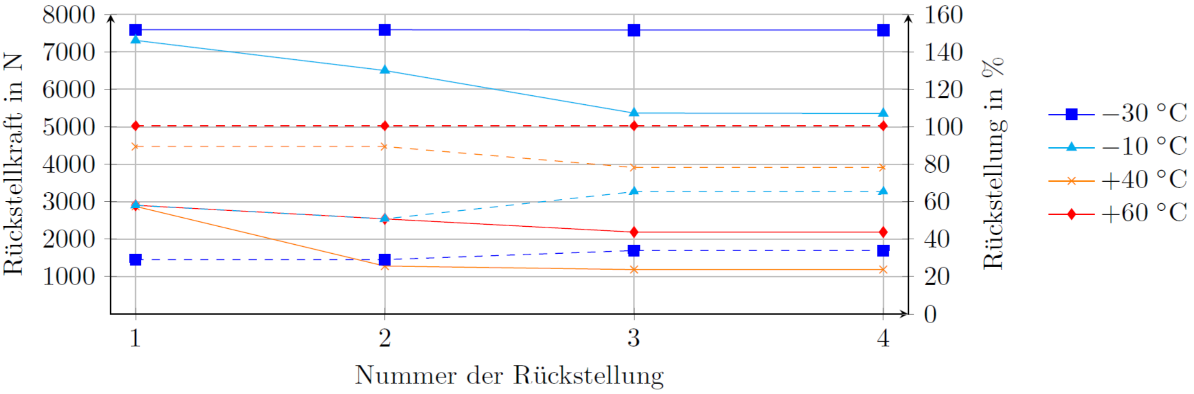

Figure 9: Results axial force measurements CF 4.0 d63/D110

4.3.2 Discussion of the results

Figure 7: Results axial force measurements CF 4.0 d32/D75 shows the results of the axial force measurements for CF 4.0 d32/D75. In this, the solid line shows the measured force, the dashed line the percentage resetting length compared to reference length. The Figure shows how the elasticity modulus decreases by increasing temperatures. Because of this, the resulting force gets smaller for higher temperatures. There is a cracking noticeable at about 95 kilograms per scale. The reset cancelled and the length kept on the length for number one in order not to destroy the pipe directly. The percentage resetting is at 44 percent at this time. The noise may be a detachment of the foam from the pipe or breakages in the insulation. For a final evaluation, and a comparison with the previous measurement of CF 2.0 d32/D75 this must be considered. The cracking is noticeable for low temperatures in all pipes. In agreement with +GF+ for further attempts, the reset shell be done until a maximum of eight kilo Newton is reached despite cracking. For a temperature of -10 °C, the initial force is approximately 2805 N and he declines hardly in the first hour. Due to the softer E-modulus with higher temperatures, the forces get smaller. For +40 °C he is about 1314 N and for +60 °C 1089 N. This is approximately a third of the force compared with -10 °C.
Test pipe and analog scale form mechanically a series connection of two springs. The spring of the analog scale has a constant of about 100 kg/cm. That means, that with a maximum force of 200 kg the pulled way of the spring is two centimeter. After resetting the test pipes to reference length, the spring of the analog scale pulls the pipe during the waiting time of one hour. This causes the pipe length during this time to change. It is observed that this phenomenon happens also for other test pipes and is in the following report called as “tensile length change”.

Figure 8 shows the results for CF 4.0 d50/D110. The forces for -10 °C and - 30 °C are the same. The reason therefore is, that for both temperatures the maximum force of eight kilo Newton is no longer sufficient to reset to reference length. By comparing the reference length with the reached length, due to eight kilo Newton traction, the percentage resetting of -10 °C is closer than -30 °C. The reached length of 995 mm for -10 °C corresponds a percentage resetting of 62 percent and the reached length of 991,5 mm for -30 °C just 35 percent. This result assumes a higher E-modulus for -10 °C.
The analog scales pulled the pipe too much for +40 °C. The percentage resetting therefore is 112 percent. This is a length of 0,2 mm for which the pipe is reset too far. On consideration between +40 °C and +60 °C, the tensile length change can be observed. That assumes a smaller force than the measured in the reality.

Finally, Figure 9 shows the results for CF 4.0 d63/D125. As expected, the maximum forces for -10 °C and -30 °C are also no longer sufficient, due to the increasing diameters. A decline of the percentage resetting shows the increasing force. For a temperature of -30 °C, the maximum force of eight kilo Newton resets to 29 percent, for a temperature of -10 °C to 51 percent. Both percentage resetting´s are lower than for CF 4.0 d50/D110. That assumes a force that is higher than for the other CF pipes. The line of the force for -10 °C declines. On the other way, the associated line of the percentage resetting increases. The reason therefore is that the length of number one hold as constant as possible. Due to tensile length change, the force was too large and has to be reduced. By resetting to 100 % for both temperatures -10 °C and -30 °C, it can be expected that it would look like the lines of CF 4.0 d50 with lower percentage for reset.
An interesting detail is that the force for +60 °C is higher than for +40 °C. The reason is increased thermal expansion resulting in a longer reset distance. Thus, despite to a softer E-modulus, the force is higher.

+GF+ compared the results with theoretically calculated data. Initially this comparison showed no matches. The measured data of the axial force test stand are for some twice as big as in the simulation model. Therefore the calculation model, especially for lower temperatures, has been adapted to depict reality.

4.3.3 Inaccuracy and measurement errors

Due to tolerances in the test stand and procedure, the following numbering explains the inaccuracy's and measurement errors:

1. **Analog scales:**
   When attaching the scales, care is taken to mount them in the most stress-free condition and to set them to "0 kg". Therefore, the nut on the threated rot is fixed until the scales hold the vertical slide beam that he can´t move anymore without producing a force. By rotating the hardness screw, which is mounted with the spring of the scale, the scale becomes set. It is necessary to repeat this procedure for each test pipe in each temperature. Because of this, the force of "0 kg" is different between each measurement.

2. **Resetting:**
   The forces of the analog scales increases by rotating the nuts on the threated rots in the same velocity and same direction. Especially for colder temperatures, the force increases a lot per millimeter. Because of this it´s not possible, to set the length to reference length by exactly this resulting force. Person one reads the reference length for a force of 4,5 kN and person two reads the reference length for a force of 5,2 kN. Actually, this variation in force measurement can`t be avoided with the current test set-up.

3. **Tensile length change:**
   The firmly clamped, installed state in systems does not permit any change in the length of the pipes. Due to the strong tensile forces and the mechanical series connection of two springs, the length of the test pipe changes between reset number one and two. At cold temperatures, the pipe becomes pulled, or at hot temperatures pressed too much compared to the force in nature. This effect causes the pipe to change his length compared with the set reset. The traction decreases, which explains most of the relaxation between reset one and two. The test set-up does not allow measuring decreasing force at a constant pipe length, what would be of interest.

4. **Force build-up:**
   A change in temperature gradually causes the resulting force. During reset, this force is applied from 0 to 100% within a few minutes. Thus the measured force is higher than the resulting one in a real installation. Point 3 describes the consequence.

5. **Permanent change in length:**
   Due to the parallel measurement of the deflection and axial force, it is only possible occasionally to approach the reference temperature in between the different set temperatures and to record a permanent change in length. It is conceivable that at 8 kN tensile force, the length of the test pipe may change from the reference length before application of the tensile force. This error is not considered.

4.3.4 Comparison with previously results

After discussing and evaluate the results, this chapter compares them with the previous measurements. Figure 10 shows the temperature on the x-scale and the force of reset number one on the y-scale.

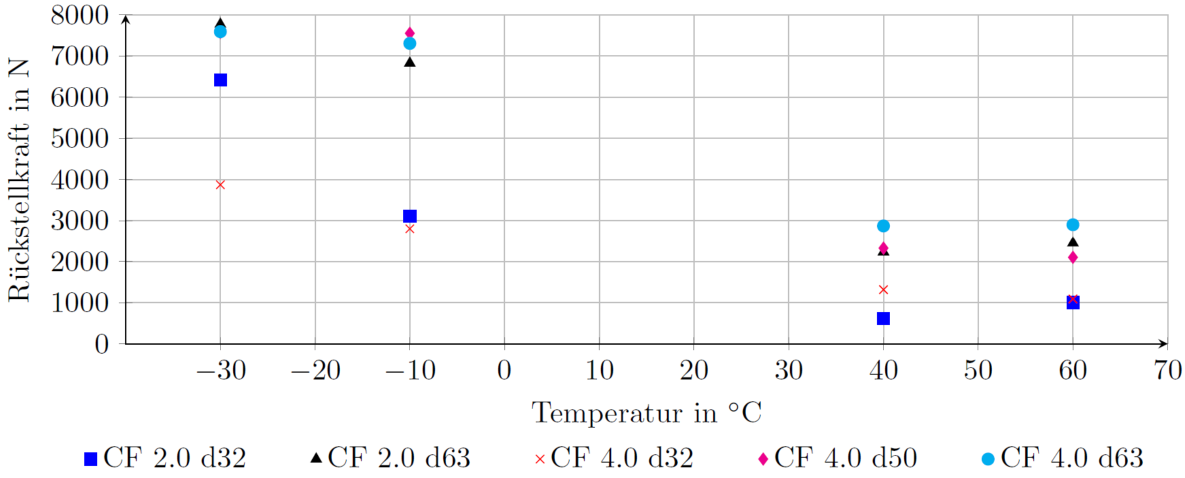

Figure 10: Comparison of Reset Number one with previous measurements

By having a look on it, it is noticeable that for -30 °C the force of CF 4.0 d32 is lower than for CF 2.0 d32. The reason therefore is the percentage reset of 44 %. As well as CF 4.0 d63, the force of CF 2.0 d63 was also not sufficient to reset to reference length. The percentage reset of CF 2.0 for -30 °C is 55 % and for CF 4.0 only 29 %. That assumes a higher resulting force for CF 4.0 due its higher diameter ratio. This can also be observed for other temperatures. The data´s of CF 4.0 are slightly larger. For example are the forces for d63 +40 °C and +60 °C approximately 1000 N higher. It was possible to reset CF 2.0 d63 to reference length for -10 °C and by 120%. This means that the measured force is too large. Anyway is the force of CF 4.0 d63 larger and the percentage reset for this temperature just 51 %. That assumes a higher difference between CF 2.0 and 4.0 by deeper temperatures.
There is no comparison of the relaxation of the force. The real decrease of it can´t be measured due to tensile length change. The decrease of the force happens not for a constant length of the test pipes.

4.3.5 Evaluation

With the determined values, it is possible to make a statement about the approximate generation of force at fixed clamped state. Accordingly, pipe clamps must withstand a force of more than 8 kN at low temperatures without being damaged. The increase in force with larger diameter ratio is evident from the comparison between Figure 7 and 8. With an increase of the inner pipe diameter by a factor of 1.56 from 32 mm to 50 mm, the force increases more than twice. Calculate an exact statement about the increase can´t be done, because 8 kN tensile force was not sufficient. It is also interesting to note that the values between +40 °C and +60 °C hardly differ in their initial value for the reset number one. The comparison with the predecessor tests brings the realization that with the same inner pipe dimension the force at CF 4.0 for warm temperatures is slightly larger than for CF 2.0. With decreasing temperature, this difference increases, so that for very low temperatures, the force on CF 4.0 pipes is significantly higher. A comparison of the force relaxation does not take place due to the tensile length change at this point. Because of the measurement inaccuracies described in Section 4.3.3, the obtained data´s serve only as a guide for further interpretations. A clear statement about the resulting force is not possible at this point.

5 L-Bent buildup measurements

5.1 Test mode

The measurement is the same than the previous measurement. The test temperatures are listed in the following table:

Table 5: Test temperatures for the L-Bent buildup measurements

Name	Target temperature	ΔT to the reference temperature
T-Positive	+60 °C	+40 K
T-Reference	+20 °C	±0 K
T-Negative	-20 °C	-40 K

The results of these and the preliminary work can be compared through the same inner diameter of the pipes. The following table compares both test pipes.

Table 6: Comparison of the test pipes

This work	Preliminary work
CF 4.0 d32/D90	CF 2.0 d32/D75
CF 4.0 d63/D125	CF 2.0 d63/D110

5.2 L-Bent buildup setup

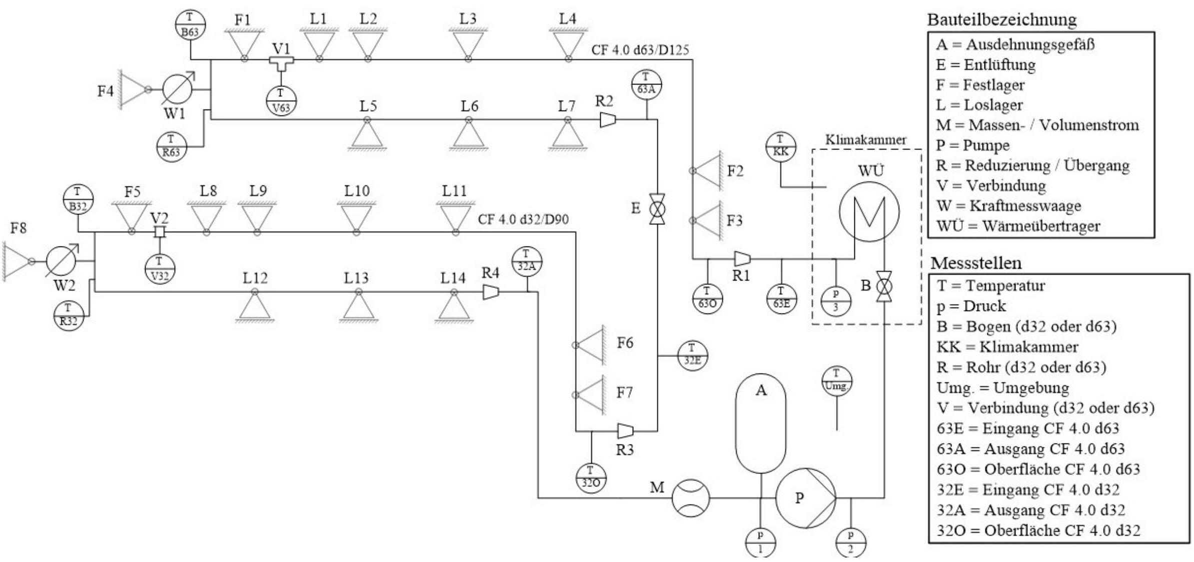

Figure 11: L-Bent buildup setup

Figure 11 shows the L-bent buildup setup. It includes all components of the test bench, which are slightly different to the structure of the predecessor. For this reason, the test stand is explained at this point. For a detailed test stand description, reference is made to the previous work. [13, p.41 ff.]

The test bench has three pressure measuring points for pressure control and monitoring. These are before and after the pump, as well as after the heat exchanger, which is located in the climatic chamber. By controlling the temperature of the climate chamber, the fluid temperature can be adjusted and controlled manually by measuring the inlet temperatures of both test pipes d32 and d63. The bend buildup, which has to be examined, is located between F2 and L4 at CF 4.0 d63, and between F6 and L11 at CF 4.0 d32. "F" refers to fixed and "L" floating bearings. Newly added is a movable bearing in front of the connector on each test tree. The reason for this is that the predecessor test bench bents at this point. This measure should prevent this. The connection (V) on test tree CF 4.0 d63 is a T-piece pointing downwards, test tree CF 4.0 d32 is an insulated welding socket. The fixed bearing after the connecting piece is used for axial clamping and holding, so when changing the fluid temperatures, due to the expansion or contraction of the lying CoolFit pipe, the resulting force presses on the bending leg and length this. F1 and F5 are fix points that can be tightened and opened with nuts. F2, F3, as well as F6 and F7 are welded and non-solvable fixed points of +GF+. On the left side of both test trees are the same analog scales used for the axial force test stand, for measuring the forces. New is a vent (E) between both test trees. This is done by a ball valve.

5.3 Measurement values

The measured values of the experiment are explained in the following not scale illustration, using the test tree CF 4.0 d63 / D125 as an example.

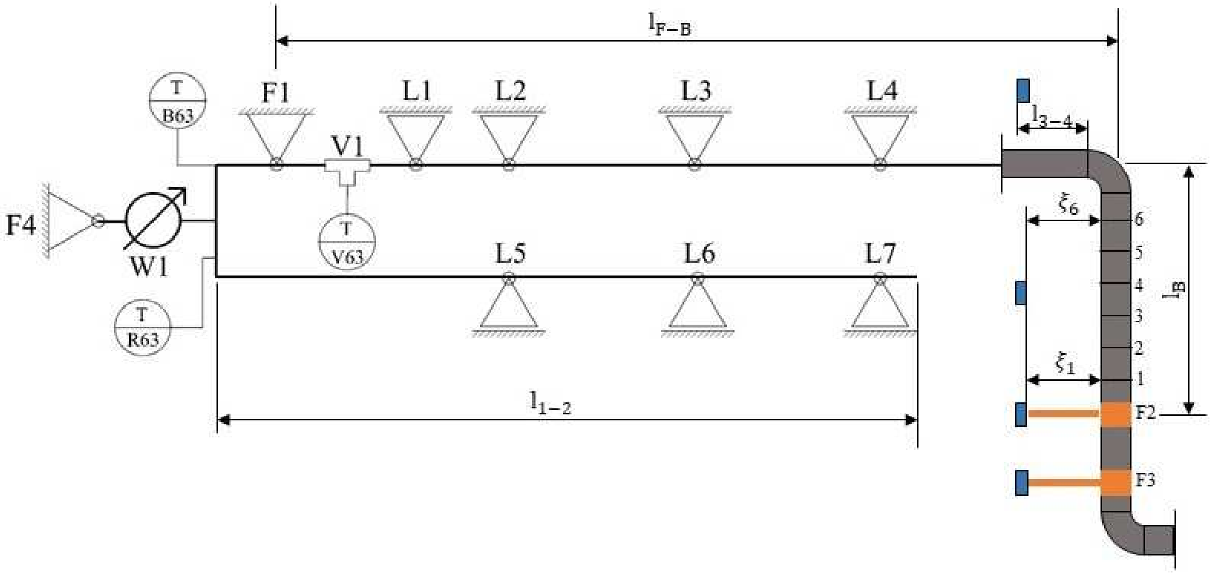

Figure 12: Measured values of the L-Bent buildup

The deflection of the L-Bent due to a change in temperature is controlled by the length l_{3-4}. This is measured by using the depth caliper presented in chapter 7.3.3 on page 30. Therefore is one wing on the inner side of the pipe shelf and a right side an angle at the edge of the sealing lip of the 90° bow. The length l_{1-2} is used to examine the free change of length of the lower, underlying CF pipe. The sealing lip of the 90° elbow and the peeled pipe edge serve as the measuring marks.

The bending leg is divided in his height from the upper fixed point (F2) to the 90° circle, into six equal parts, which are marked on the pipe. These are schematically drawn in the Figure 12. A bending line can be measured to show deflections and provisions graphically due this dividing.

5.4 Test procedure

The test procedure is the same as from the predecessor. Because of increasing diameter ratios is it necessary to change one detail. Point 12 becomes instead of 10 cm only 5 cm bent.

1. Set the climate chamber to a fluid temperature of 20 °C at the inlet to CF 4.0 d63 about night.
2. Open the fixed points F1 and F5 and set the L-Bend to a 90°-position. Control about a spirit level.
3. Measuring of p_1 until p_3, l_{1-2}, l_{3-4} and the bending line through measuring of ξ_1 until ξ_6.
4. Set the target temperature
5. When medium- and surface temperatures constant: repeat number 3 at target temperature
6. Calculation of thermal expansion through the difference of l_{3-4} at target and reference temperature.
7. Opening the fix points F1 and F5.
8. Set the L-bend back to a 90°-position. Control about measured l_{3-4} from number 3.
9. Set the analog scales to “0 kg”.
10. Bending the L-Bent in the direction of thermal expansion by the calculated difference of number 6. Control via l_{3-4}.
11. Measuring from l_{3-4} and the bending line through ξ_1 to ξ_6, as well as the force of the analog scale.
12. Bending of the L-bent in the direction of thermal expansion for a length of 5 cm.
    → $l_{3-4,\ Number\ 12,\ target} = l_{3-4,\ Number\ 3} \pm 5\ cm$
13. Measuring of l_{3-4}, the bending line ξ_1 until ξ_6 and the force of the analog scale.
14. Waiting for one hour.
15. Relaxation: Measuring of l_{3-4}, the bending line ξ_1 until ξ_6 and the force of the analog scale.
16. Repeat Point 8 until 15 with the difference of all deflections in the opposite direction compared to thermal expansion (bending left, bending right)

5.5 Results

5.5.1 Temperature recordings

Before the measurement results are considered, the temperature records should be briefly displayed.

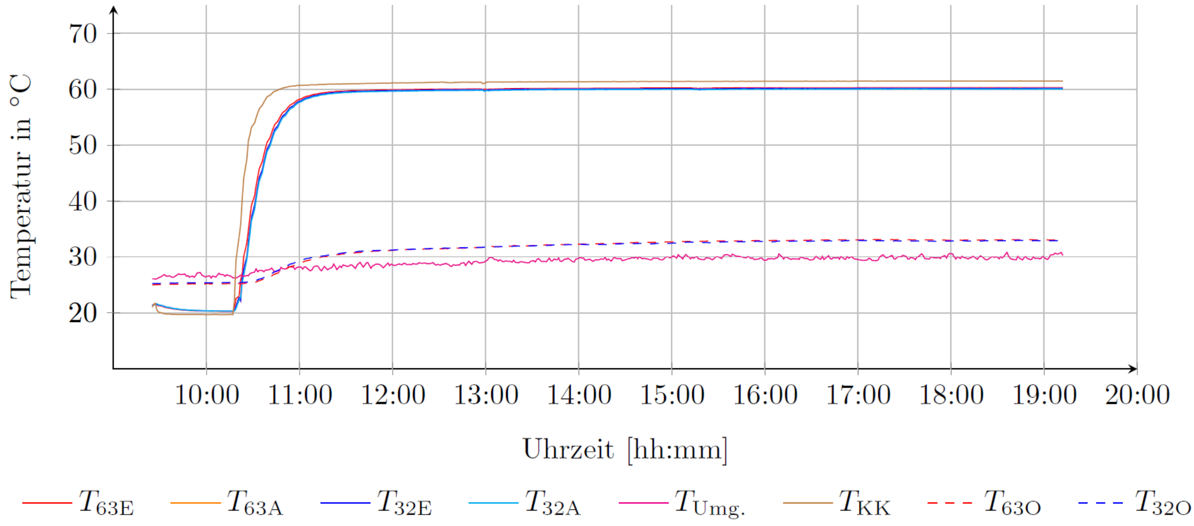

Figure 13: Temperature recording, Medium +60 °C

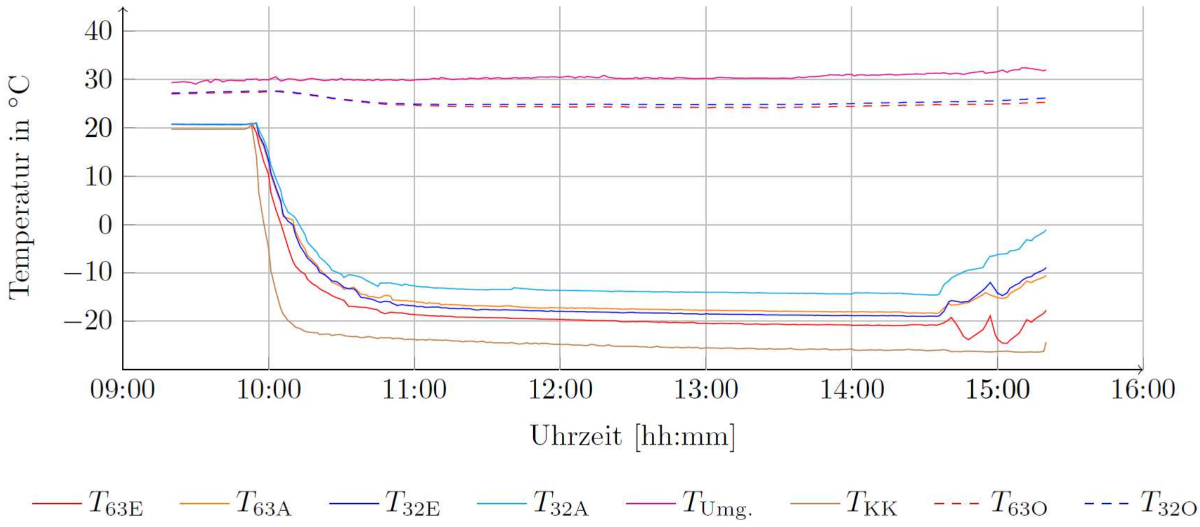

Figure 14: Temperature recording, Medium -20 °C

Figure 13 shows the temperatures plotted with the time on the x-axis about the temperature recordings of the inserted sensors. For the target temperature of +60 ° C, the test medium water is used as the refrigerant. Water, as shown in the figure, takes quickly the temperature of the climatic chamber. All measured fluid temperatures are constant and almost exactly +60 °C.

Figure 14 has a propylene glycol / water mixture due to the cold temperatures as refrigerant. The mixing ratio is approximately 70/30. The target temperature of -20 °C is set for the input in the pipe d63. In a first comparison with Figure 13, it can be observed that the temperatures of the PG / W mixture differ significantly between the individual measuring points. This can be attributed to the higher viscosity for cold temperatures and the associated poor pump ability of the pump. This phenomenon was also observed in the previous work. At about 15:00, the pump makes strange noises. The pump was switched off and follow-up tests can’t be done. This explains why at -20 ° C only left measurements are made.

5.5.2 CF 4.0 d32/D90

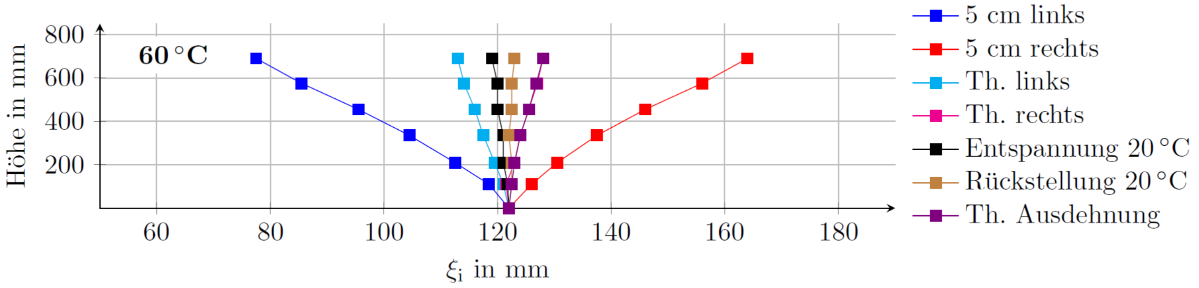

Figure 15: Bending line CF 4.0 d32/D90 for +60 °C

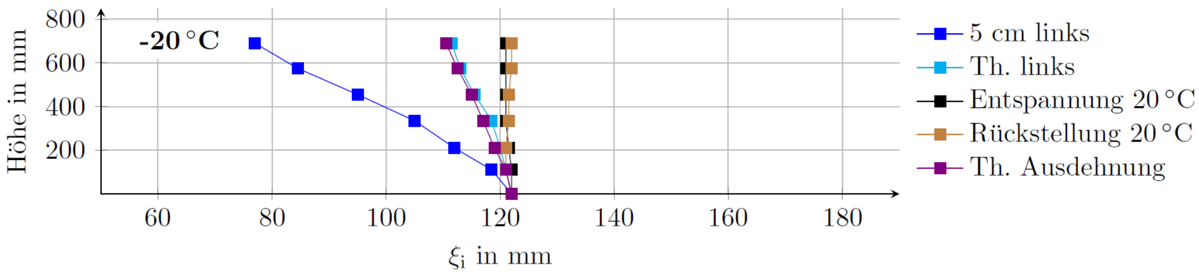

Figure 16: Bending line CF 4.0 d32/D90 for -20 °C

Figure 15 and 16 shows the measured bending lines of the L-bend buildup. They visualize and check the resets and deflections. As example, Figure 16 shows the accordance between the 90°-positon for target and reference temperature. Both bending lines are almost on top of each other. The same applies to the thermally induced deflection. This is recorded in each case after the tempering (Th. Ausdehnung) and set again after the return to 20 °C-position with the analog scales to be able to obtain the resulting force. Both bending lines (Th. Extension and Th. Left) are nearly on top of each other and are also well adjusted. By comparing Figure 15 and Figure 16, the contraction and expansion of the materials can be observed. For temperatures higher than 20 °C, the materials expand, the resulting deflection presses on the bending leg and lengthens it. For this reason the bending line for the thermal expansion runs to the right at +60 °C. At -20 °C, the resulting force pulls on the bending leg due to the contraction and extends it to the left, as well as the course of the bending line.

Figure 17 shows the measured forces for the bending of the showed bending lines. “Δl_{3-4}” shows the force induced thermally. Therefore, the according bending line is the setting of "Th. Links" and "Th. Rechts". The corresponding solution tables show the measured data´s. "5 cm" is the exaggerated deflections "5 cm links" and "5 cm rechts". Last measure indicates the relaxation of the force of "5 cm".

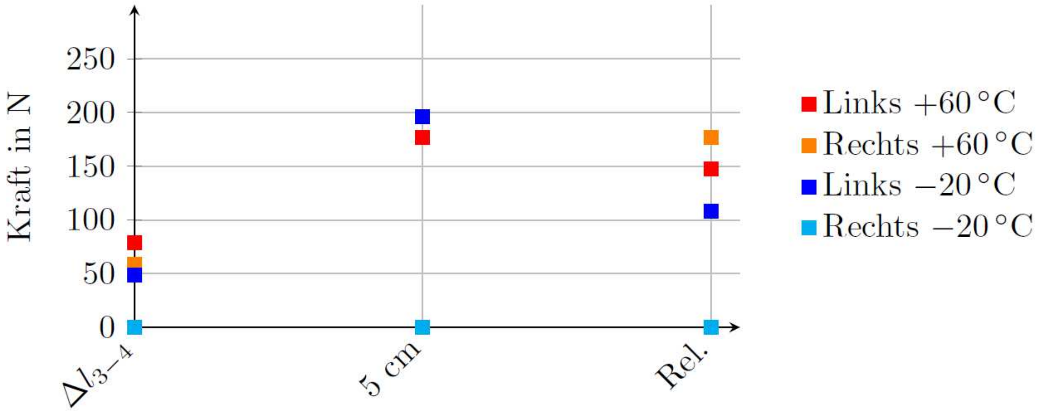

Figure 17: Measured forces for test pipe d32

Table 7 and Table 8 show the measurements for +60 °C and -20 °C. Therein the set for the deflection can be compared. From the difference between relaxation at +20 °C (Relax) and the thermally induced deflection (Thermal) at the target temperature results the reference value l_{3-4} for the left and right side. F_B (N) is the measured force as plotted in Figure 17: Measured forces for test pipe d32.
The force values for right deflections at -20 °C could not be recorded due to the defective pump. Because of this, they are all zero. The measured force values of the thermally induced deflection and the coated deflection of 5 cm hardly differ for all temperatures. Only in the relaxation, small differences are measured. At a temperature of -20 °C, the force in the loaded hour decreases by about 50 %. This relaxation is much smaller for +60 °C. For the thermal deflection, there is a maximum force of <80 N, for the excessive "5 cm" deflection the force is nearly 200 N.

Table 7: Results L-Bend buildup CF 4.0 d32 for +60 °C

-	Relax	Thermal	Reset	Th. Left	Th. Right	5 cm left	5 cm right
l_{3-4}	14,85 cm	15,90 cm	14,85 cm	13,85 cm	15,90 cm	9,85 cm	19,90 cm
Δl_{3-4}	0,00 cm	1,05 cm	0,00 cm	-1,00 cm	-1,05 cm	-5,00 cm	5,05 cm
F_B	-	-	-	78,48 N	58,86 N	176,58 N	196,20 N

Table 8: Results L-Bend buildup CF 4.0 d32 for -20 °C

-	Relax	Thermal	Reset	Th. Left	Th. Right	5 cm left	5 cm right
l_{3-4}	14,96 cm	13,72 cm	15,00 cm	13,70 cm	-	10,00 cm	-
Δl_{3-4}	0,00 cm	-1,24 cm	0,04 cm	-1,26 cm	-	-4,96 cm	-
F_B	-	-	-	49,05 N	-	196,20 N	-

5.5.3 CF 4.0 d63/D125

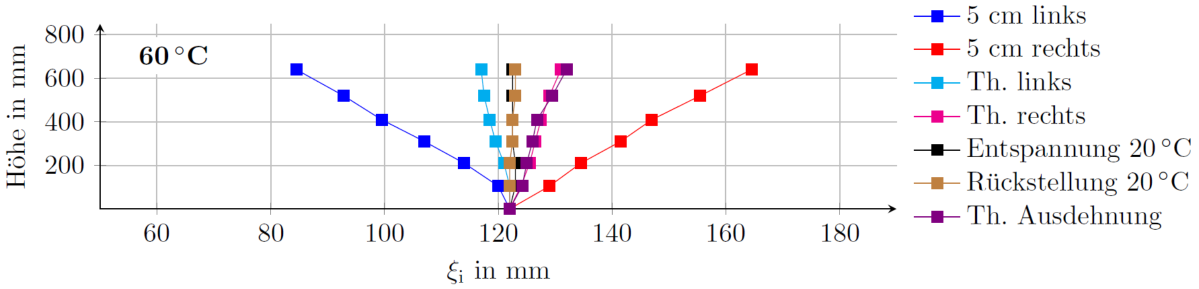

Figure 18: Bending line CF 4.0 d63/D125 for +60 °C

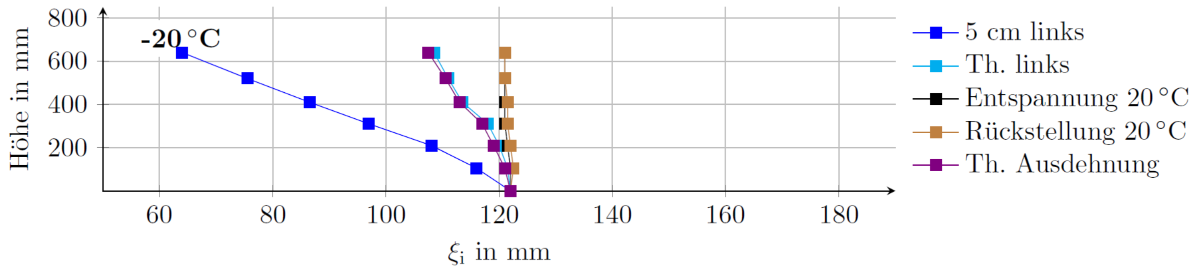

Figure 19: Bending line CF 4.0 d63/D125 for -20 °C

Figure 18 and Figure 19 shows also the bending lines, but for CF 4.0 d63. The thermally induced elongations are adjusted very well for -20 °C and at +60 °C. The coated deflection at -20 ° C is too large compared to +60 °C. The deflection for -20 °C of 6.07 cm was calculated with the thermally induced deflection and not with l_{3-4} at +20 °C. A striking error when looking at the bending lines. For a comparison of forces, this must be taken into account. As with the recorded bending lines for CF 4.0 d32, the direction of the deflection can also be observed with CF 4.0 d63 by considering the "Th. Expansion".

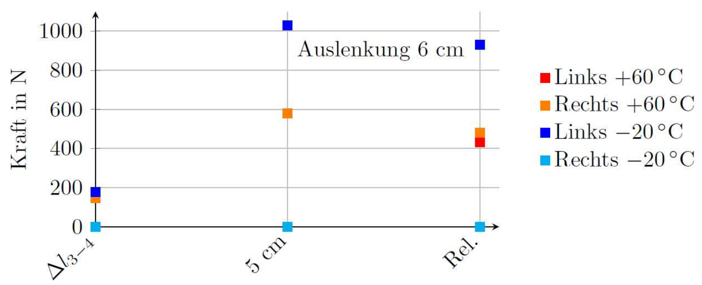

Figure 20: Measured forces for test pipe d63

The measured forces of the thermally induced deflection differ slightly. With a maximum of 180 N and a minimum of 150 N are they 30 N apart. The exaggerated deflection shows differences in the forces, which happens not only due to the deflection of 6 cm but also due to an increased modulus of elasticity for cold temperatures. An increase from 580 N at +60 °C to 1030 N at -20 °C corresponds to an increase of 77,5 %. This increase is not related to the thermally induced force and the increase to the excessive 5 cm deflection at + 60 °C. When looking at the surface temperatures from chapter 5.5.1, it is clear that they do not change significantly due to the change in the fluid temperature. The modulus of elasticity of the outer pipe can therefore be assumed to be the same for all measurements. Only the modulus of the inner pipe changes, because it comes into direct contact with the medium. Such an increase must be confirmed with comparative measurements. As already seen, the forces between warm and cold temperatures are not significantly different.

Table 9: Results L-Bend buildup CF 4.0 d63 for +60 °C

-	Relax	Thermal	Reset	Th. Left	Th. Right	5 cm left	5 cm right
l_{3-4}	16,60 cm	17,50 cm	16,65 cm	15,70 cm	17,45 cm	11,70 cm	21,60 cm
Δl_{3-4}	0,00 cm	0,90 cm	0,05 cm	-0,90 cm	0,85 cm	-4,90 cm	5,00 cm
F_B	-	-	-	176,58 N	147,15 N	578,79 N	578,79 N

Table 10: Results L-Bend buildup CF 4.0 d63 for -20 °C

-	Relax	Thermal	Reset	Th. Left	Th. Right	5 cm left	5 cm right
l_{3-4}	16,07 cm	15,02 cm	16,10 cm	15,10 cm	-	10,00 cm	-
Δl_{3-4}	0,00 cm	-1,05 cm	0,03 cm	-0,97 cm	-	-6,07 cm	-
F_B	-	-	-	176,58 N	-	1030,05 N	-

5.5.4 Comparison of all results

When considering the results, care must be taken that the deflection, in Figure 16 and 17 with "Ausl." abbreviated, for all CF 2.0 pipes amounts to 10 cm, for CF 4.0 amounts to only 5 cm.

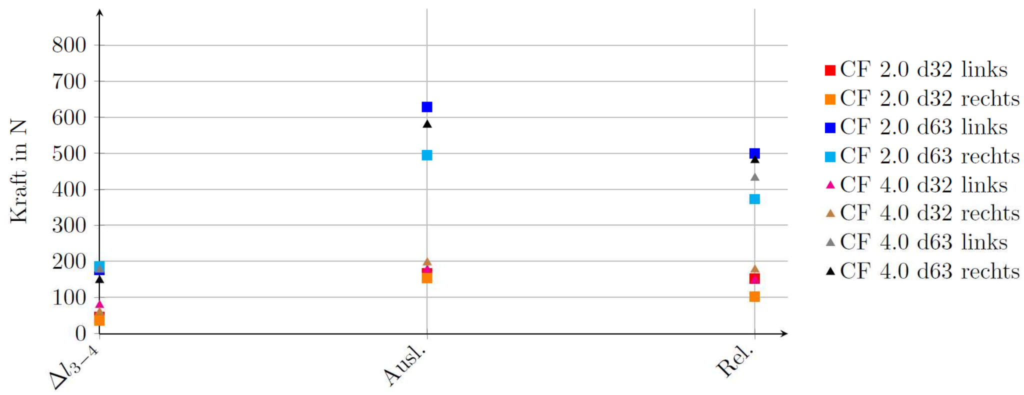

Figure 21: Comparison with privious tests for +60 °C

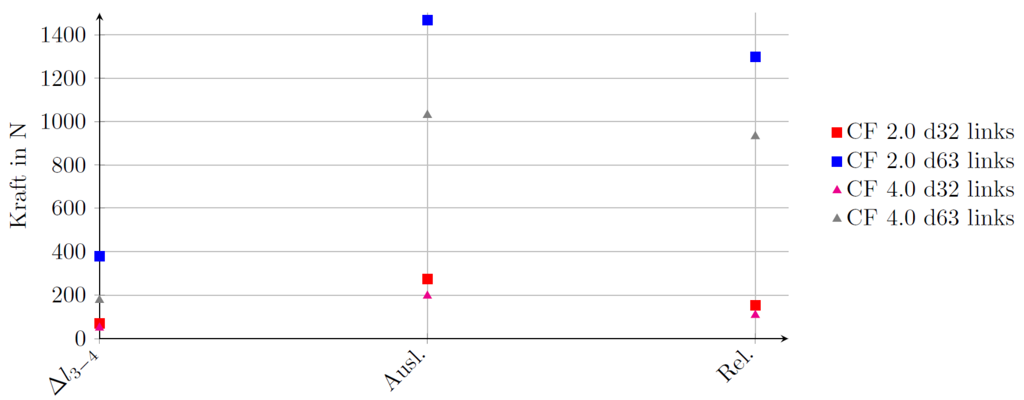

Figure 22: Comparison with privious results for -20 °C

The measurement of the resulting bending forces due to temperature change can be compared directly with each other. The art of measurement corresponds to preliminary work. The comparison shows that the forces of the pipe d63 are the same as expected. Differences can be found between CF 2.0 and CF

4.0. Only CF 2.0 d63 at -20 °C is lower than the other specimens. The measured values of preliminary work are listed in Tables 11 to 14.

The comparison of the exaggerated deflection is more complex due to different deflection. The forces of CF 4.0 are lower than for CF 2.0. For +60 °C, this difference is much smaller compared with -20 °C. There are two reasons, which explain the increasing. Due to higher E-modules of the inner pipe, the forces become too strong at -20 °C. The comparison of both temperatures shows these significant increases in force at cold temperatures. Second reason is that, due to increasing diameter ratio, the forces increase. Because of this, the exaggerated bending of 5 cm for CF 4.0 needs almost the same force than 10 cm for CF 2.0.

Table 11: Results L-Bend buildup CF 2.0 d32 for +60 °C

-	Relax	Thermal	Reset	Th. Left	Th. Right	10 cm left	10 cm right
l_{3-4}	11,60 cm	12,58 cm	11,60 cm	10,35 cm	12,85 cm	1,60 cm	21,90 cm
Δl_{3-4}	0,00 cm	1,25 cm	0,00 cm	-1,25 cm	1,25 cm	-10,00 cm	10,30 cm
F_B	-	-	-	46,60 N	36,79 N	166,77 N	154,51 N

Table 12: Results L-Bend buildup CF 2.0 d63 for +60 °C

-	Relax	Thermal	Reset	Th. Left	Th. Right	10 cm left	10 cm right
l_{3-4}	11,00 cm	12,70 cm	11,00 cm	9,50 cm	12,50 cm	1,00 cm	21,00 cm
Δl_{3-4}	0,00 cm	1,70 cm	0,00 cm	-1,50 cm	1,50 cm	-10,00 cm	10,00 cm
F_B	-	-	-	176,58 N	186,39 N	627,84 N	495,41 N

Table 13: Results L-Bend buildup CF 2.0 d32 for -20 °C

-	Relax	Thermal	Reset	Th. Left	Th. Right	10 cm left	10 cm right
l_{3-4}	11,60 cm	10,05 cm	11,60 cm	10,05 cm	13,15 cm	1,60 cm	21,60 cm
Δl_{3-4}	0,00 cm	-1,55 cm	0,00 cm	-1,55 cm	1,55 cm	-10,00 cm	10,00 cm
F_B	-	-	-	70,31 N	40,88 N	274,68 N	196,20 N

Table 14: Results L-Bend buildup CF 2.0 d63 for -20 °C

-	Relax	Thermal	Reset	Th. Left	Th. Right	10 cm left	10 cm right
l_{3-4}	11,00 cm	9,00 cm	11,00 cm	9,00 cm	13,00 cm	1,00 cm	21,00 cm
Δl_{3-4}	0,00 cm	-2,00 cm	0,00 cm	-2,00 cm	2,00 cm	-10,00 cm	10,00 cm
F_B	-	-	-	379,32 N	235,44 N	1466,60 N	925,41 N

Table 15: Overview about the resets of the L-Bend buildup

Temp.	Test pipe	$\Delta l_{3-4,th.}$	$\Delta l_{3-4,left}$	$\Delta l_{3-4,right}$	$\Delta l_{3-4,exag.left}$	$\Delta l_{3-4,exag.right}$
+60 °C	CF 2.0 d32	1,25 cm	-1,25 cm	1,25 cm	-10,00 cm	10,30 cm
	CF 2.0 d63	1,70 cm	-1,50 cm	1,50 cm	-10,00 cm	10,00 cm
	CF 4.0 d32	1,05 cm	1,00 cm	1,05 cm	-5,00 cm	5,05 cm
	CF 4.0 d63	0,90 cm	-0,90 cm	0,85 cm	-4,90 cm	5,00 cm
-20 °C	CF 2.0 d32	-1,55 cm	-1,55 cm	1,55 cm	-10,00 cm	10,00 cm
	CF 2.0 d63	-2,00 cm	-2,00 cm	2,00 cm	-10,00 cm	10,00 cm
	CF 4.0 d32	-1,24 cm	-1,26 cm	-	-4,96 cm	-
	CF 4.0 d63	-1,05 cm	-0,97 cm	-	-6,07 cm	-

5.5.5 Evaluation

For the warm temperature of the medium, which is +60 °C, water turns out to be well suited due to the large heat transfer. The temperatures can be adjusted easily and constantly. In order to avoid freezing of water at low temperatures and to protect components from destruction, a propylene glycol / water mixture is used. The PG/W mixture can´t promoted as good as water and has a lower heat transfer, which is shown by the temperature recordings due to larger differences compared with water. Setting a constant fluid inlet temperature turns out to be more complex or not possible.

When assessing the measurement results, the forces due to the thermal deflection show agreement with the previous tests. For the exaggerated one can´t be determined any definite tendency. In the previous experiments, a mean value is formed from several measurements and used for the comparisons. The measurements carried out in this work are based on only one measurement per temperature. For this reason, no verification of the results can be done, because no comparative measurements have been carried out. The pump failure also caused a premature termination of the measurements.

6 Thermally induced change of length

6.1 Test mode

As a result of temperature changes, there is a thermally induced change in length for all materials. [14, p.18]

The following tests will investigate different multilayer pipes of +GF+ and compare them with a PE-100 reference pipe. For this purpose, the lengths of the inner and the outer pipe at -50 °C, +20 °C and +70 °C are documented. From these lengths, a thermal expansion coefficient α_{Rohr}, as well as an expansion per meter of pipe length ΔL can be calculated. All test pipes have an approximate length of one meter and are of dimension d110.

6.2 Test pipes

CoolFit 2.0, as well as CoolFit ABS has been studied in previous work on their thermal expansion. The test pipes examined in this work differ in their construction from CoolFit and should be explained in their structure.

The test pipes are from the "ecoFIT-stiff pipe" product class, which is made up of three different polyethylene layers. For this reason, they are also referred to as three-layer pipes. They exhibit high impact strength and good chemical abrasion resistance within a wide temperature range from -50 °C to +60 °C. In all pipes, the core layer is glass fiber reinforced. The following pipes are used for the experiment:

1. **PE-GF 2.5 V3a:**
   Pipes from the class 2.5 V3a are equal in their layer thickness distribution to V3b. It consists of a 3.33 mm inner layer, a 3.33 mm core layer and a 3.33 mm outer layer. In addition, they have a glass fiber content of 20 wt.-% of the compound of the core layer. V3a differs from V3b in it´s not pre-dried during production.

2. **PE-GF 2.5 V3b:**
   The structure and the layer thickness distribution correspond to the same of V3a pipes. However, this variant is pre-dried during production. The background is a type of bubble formation in the glass-fiber reinforced polyethylene layer during extrusion, which can be caused by water absorption of the pellets. For this reason, the pellets are pre-dried in an oven before being extruded.

3. **PE-GF 2.7 V5:**
   Class 2.7 pipes have a different layer thickness structure. With glass fiber content of 30% they are 10 wt.-% higher than class 2.5. The layer thickness distribution is the same as for the pipes of class 2.5. It consists of a 3.33 mm inner layer, a 3.33 mm core layer and a 3.33 mm outer layer.

4. **PE-GF 2.7 V6:**
   Variant 6 differs by the layer thickness distribution of the variant V5. This consists of a 4.99 mm inner layer, a 3.33 mm core layer and a 1.66 mm outer layer.

5. **PE-100 reference:**
   The reference pipe is PE-100 d110, which is made of polyethylene. However, this does not have multiple layers and has a wall thickness of 10 mm. It´s used to have the possibly to compare the results of different layer structures.

6.3 Test procedure

The four test pipes, the PE-100 reference pipe, a borosilicate glass rod and the tape measure are stored in the climatic chamber and tempered overnight to + 20 °C. In the morning, the lengths on the inner and outer pipe are documented and the climate chamber is switched to +70 °C during the day, so that in the evening the new lengths can be measured at a new temperature. Temperatures of +70 °C and -50 °C are not sustainable for the human body, so the measurements are being carried out quickly. In order to exclude measurement errors, the measurement is repeated after one hour and the measured values are compared with each other. During the night, a temperature of +20 °C is set again so that the temperature can be adjusted to -50 °C during the day. The borosilicate glass rod has a very linear and constant coefficient of thermal expansion, as already investigated in previous work. The extent of the actual measuring instrument due to the temperature change can be taken into account with its help. Following numbering describes the test procedure in summary:

1. Tempering to +20 °C about night.
2. Measuring of the length at the inner- and outer pipe, as well as the borosilicate glass rod.
3. Tempering to target temperature number one while the day.
4. Repeat point two at about 16:30.
5. Waiting for one hour and repeat point two at about 17:30.
6. Tempering to +20 °C about night.
7. Repeat point two.
8. Tempering to second target temperature while the day.
9. First measurement at about 16:30.
10. Second measurement after one hour waiting at about 17:30.

6.4 Evaluation

The calculation process for the evaluation is shown schematically in the appendix chapter A.3 on page 70 in the German version. The following values result from Table 16 and Table 17. For a better overview the final results are summarized in Figure 23.

Table 16: Results of the thermal change of length calculation for +70 °C

Type	Structure	Thermal expansion coefficient		ΔL	
2.5	V3a	$\alpha_{m,V3a}$	5,795E-05 1/K	ΔL_{V3a}	2,897 mm/m
	V3b	$\alpha_{m,V3b}$	6,042E-05 1/K	ΔL_{V3b}	3,021 mm/m
2.7	V5	$\alpha_{m,V5}$	3,398E-05 1/K	ΔL_{V5}	1,699 mm/m
	V6	$\alpha_{m,V6}$	4,050E-5 1/K	ΔL_{V6}	2,025 mm/m
Ref.	PE-100	$\alpha_{m,Ref.}$	1,668E-04 1/K	$\Delta L_{Ref.}$	8,338 mm/m

Table 17: Results of the thermal change of length calculation for -50 °C

Type	Structure	Thermal expansion coefficient		ΔL	
2.5	V3a	$\alpha_{m,V3a}$	6,762E-051/K	ΔL_{V3a}	-4,733 mm/m
	V3b	$\alpha_{m,V3b}$	8,681e-05 1/K	ΔL_{V3b}	-6,076 mm/m
2.7	V5	$\alpha_{m,V5}$	6,549E-05 1/K	ΔL_{V5}	-4,584 mm/m
	V6	$\alpha_{m,V6}$	6,267E-05 1/K	ΔL_{V6}	-4,387 mm/m
Ref.	PE-100	$\alpha_{m,Ref.}$	1,174E-04 1/K	$\Delta L_{Ref.}$	-8,216 mm/m

It is noticeable that the PE-100 reference pipe reacts more strongly to temperature changes, than the multi-coated pipes. With an increase of 8,54 mm/m at +70 °C it reacts more than four times greater than PE-GF 2.7 V5. This pipe reacts hardly to the temperature rise, only by 1,699 mm/m. Of the three-layer pipes, the increase in PE-GF 2.5 is the largest. The data´s are almost the same, which are 3,1 mm/m for V3a and 3,2 mm/m for V3b. The same behaviour is also seen for cold temperatures, with the difference that the pre-dried variant V3b contracts more than the not pre-dried V3a. This value is the largest with a length decrease of -6,09 mm/m. Only the PE-100 reference pipe is even larger and is calculated to -8,23 mm/m. The behaviour of the pipes can be explained by their structure and corresponds to the expectations. Class 2.7 pipes are the least sensitive to temperature changes due to the higher glass fiber content. Pipes of class 2.5 are 10 wt.-% less than class 2.7. The reference pipe does not have glass fiber reinforcement and therefore reacts more to temperature changes. It is also noticeable that PE-GF 2.7 pipes show the same behaviour with very little difference in warm and cold temperatures. As a result, it can be said that the glass fibers must be aligned longitudinally. Only this orientation explains the big difference between the pipes.

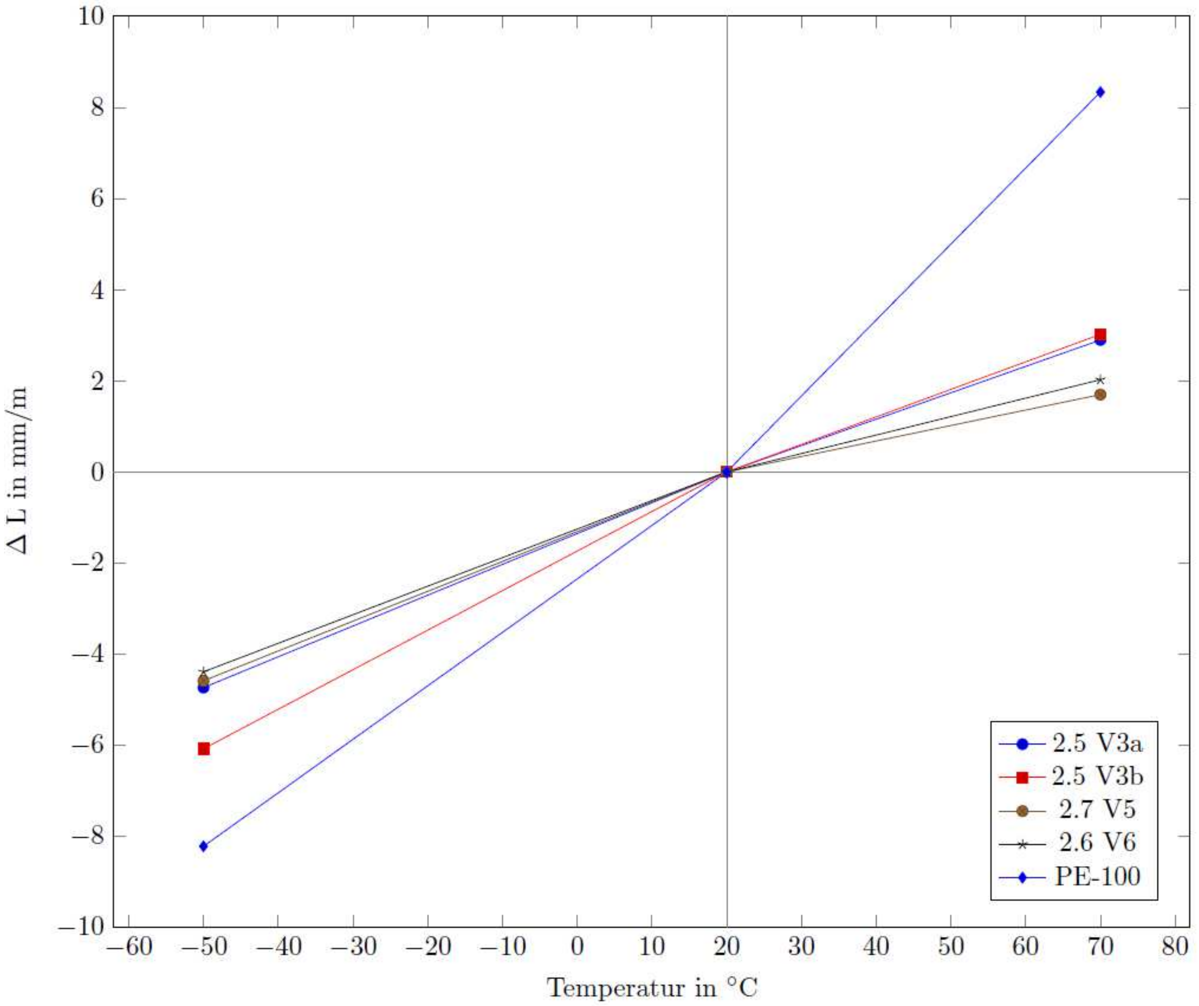

Figure 23: Expansion and contraction of multi-layer pipes

7 Time dependent deflection behaviour

7.1 Test mode

The aim is to investigate the time-dependent creep from test pipes to bending stress at different temperatures. For this purpose there are pre-insulated, as well as single pipes, which have the inner pipe dimension d32. A centrally mounted single load realizes the bending stress. The documentation of the increase in deflection and the time should provide information about the modulus of elasticity of the material, from which further conclusions can be derived. The following pipes are used for the experiment:

- CF 2.0 d32/D75
- CF 2.0 d32/D75 with central fitting
- CF 4.0 d32/D90
- CF 4.0 d32/D90 with central fitting
- CF ABS d32/D90
- CF ABS d32/D90 with central fitting
- Single pipes: PB-H, ABS, PVC-C, PVC-U, PE-100, PP-H

Due to their greater inherent stability, CoolFit pipes should have a span of three meters, whereas simple pipes only have half of them.

7.2 Time dependent behaviour of polymers by constant stress

Polymers can withstand greater elastic strains before plastic deformation remains compared with metals. If they are subjected to a tension, which is below the yield stress occurs a strain that increases with time. When the voltage is applied, as it jumps from zero to σ, the strain increases to an initial ϵ_0 before the increasing gets lower. The constant stress time-dependent modulus of elasticity $E_c(t)$ is defined as follows: [15, p.268]

$$E_c\,(t) = \frac{\sigma}{\epsilon(t)} \tag{7-1}$$

The deformation and also $E_c(t)$ strive for a constant value for large times. After removing the load at time *t*, the strain decreases abruptly by the non-time-dependent amount ϵ_0 and returns then to zero. The retardation time τ_{Ret} is defined as the time at which the time-dependent portion of the strain has decreased to 1/e times the original value. Figure 24 shows the creep behavior after applying and keeping a constant stress for polymers.

For the evaluation of the creep properties, the creep resistance index c_c should be introduced. He describes the temporal decrease of the material stiffness. The larger the index, the smaller the creep. The creep resistance can assume a maximum value of $c_c = 1$. Such a material has a temporally constant rigidity. The definition of the measure is shown in the following equation, where E_{c0} equals $E_c(t = 10^0\ h)$ and E_{c3} equals $E_c(t = 10^3\ h)$: [16]

$$c_c = \frac{E_{c3}}{E_{c0}} \tag{7-2}$$

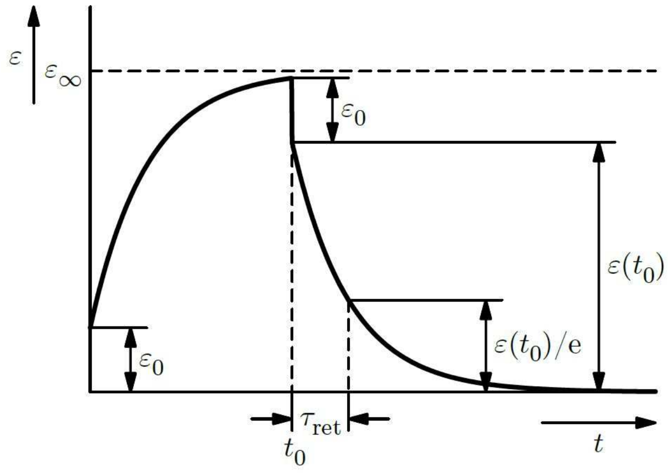

Figure 24: Creep behaviour by constant stress for polymers [15, p.268]

7.3 Teststand

7.3.1 Total Construction

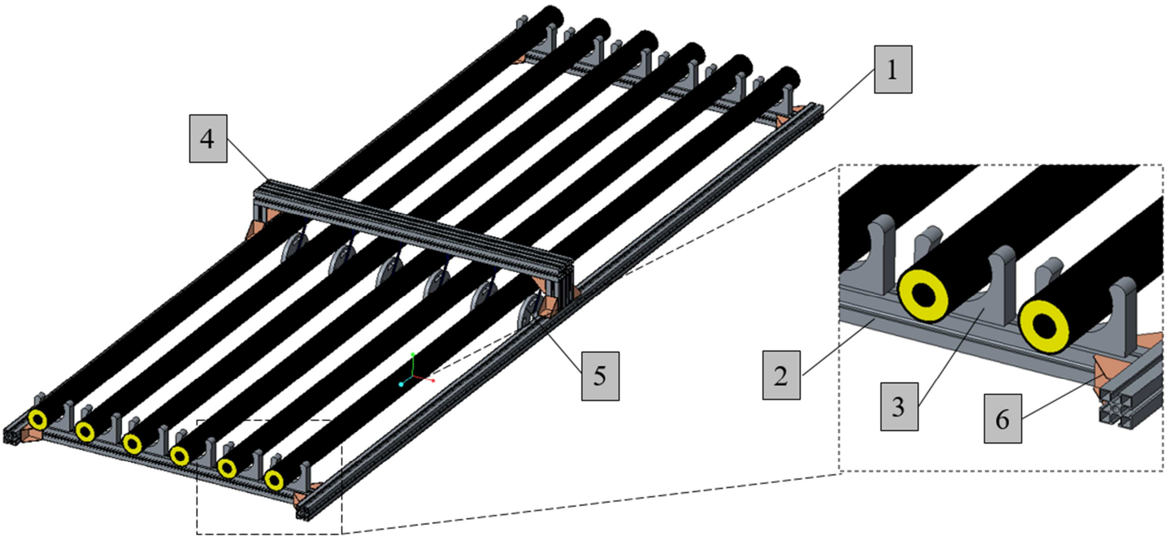

Figure 25: CAD Construction to measure the time-dependend deflection

There are different elements in the construction. First of all, the frame elements guide profile {1} and setting Profile {2}. So-called "clip-it" holders from +GF+ {3} hold the pipes. They are in larger dimension than the test pipe, so that it can bend freely. In the middle of the frame construction, there are two identical bridges {4}. These are mounted parallel with an interval of a few millimeters, so that the pipe deflection can be measured with a depth measurement (chapter 7.3.3). Below the bridge, the test weights {5}, as presented in chapter 7.3.2, are schematically shown. Due to the fact, that simple pipes are tested at a different distance of the clip-it holders than CoolFit pipes, the setting profiles of the frame are connected to the guide profile by fixing brackets {6}. By opening the connecting screws the distance can be adjusted. Attached markings on the guide profile allow a quick change of the span.

7.3.2 Test weights

For the test weights there are weight plates used, which has a single weight of about 1270 g. They have a central bore and are connected by a threaded rod. On this are nuts as balancing weights. With a screwed eyelet, the weights get into hooks that hang with cable ties or chains around the test pipes. In order to obtain measurable deflections, test weights with a total weight of five kilograms are sufficient for CooFit pipes and 2.5 kg for single pipes. The design can be found in the appendix, chapter A.4, page 72 of the German edition. The designed test weights serve as reference. The weight must be adjusted depending on the temperature. For soft samples the weight is reduced and increased for hard samples. The following two figures show the test weights.

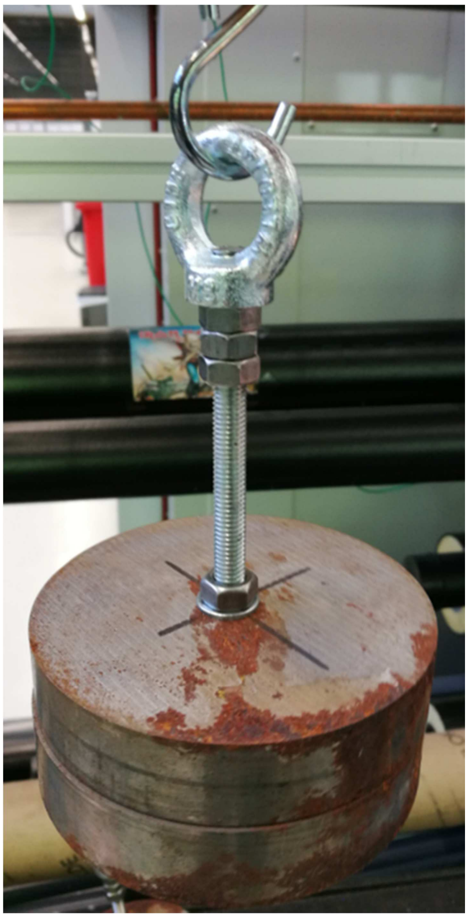

Figure 26: Test weight without mounting

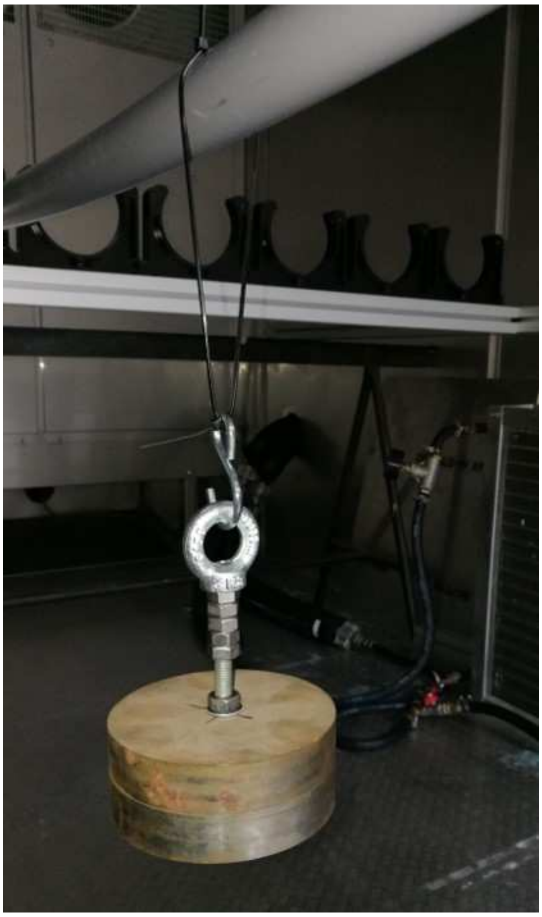

Figure 27:Test weight mounted

7.3.3 Deflection measurement

The ”bridge” {4} is necessary to measure the time-dependent deflection and described in the following figure.

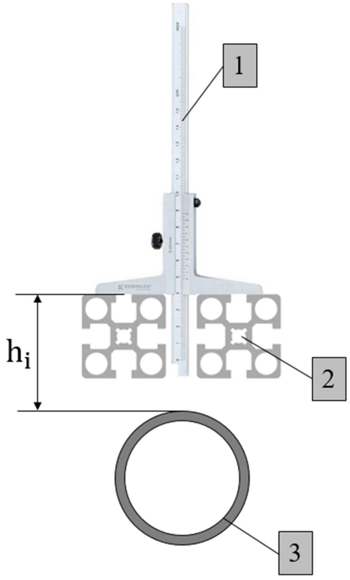

Figure 28: Measuring of the deflection

Figure 28: Measuring of the deflection shows a section through the bridge from Figure 25. In addition to the depth caliper {1}, there is also the bridge of Minitec profiles {2} and the test pipe {3}. The bridge has a small gap in the middle. The caliper can be extended in it and measure the depth h_i. As a measuring instrument, a depth caliper is selected because it rests on both sides by the wings. This ensures that the deflection is measured vertically and at each measurement at the exact same angle. In addition, it is possible to read the deflection to the nearest tenth of a millimeter. The depth h_i is the dimension from the top of the bridge to the top of the test pipe. To capture a deflection ϵ_i of the test pipe, it is necessary to measure a reference $h_{Referenz}$ without a weight and subtract it from its depth h_i.

That means in equation:

$$\epsilon_i(t) = h_i(t) - h_{Referenz}(t = 0\ s) \tag{7-3}$$

Therein describes “i” any measured time. “$Referenz$” describes the height without any load.

7.3.4 Thermal induced error

Each material changes his length due to temperature changings. The measured deflection should be compared by a measured reference length, which would be measured if the caliper has a core temperature from 20 °C. The Problem is that the caliper lies for the whole time of the test in the climate chamber and take the same core temperature than the test pipes. Because of this he change his length and the measured length are false. If the test pipe is loaded at temperatures below 20 ° C, the length of the depth caliper will contract and the value of the caliper h_i will increase. If the test temperature is higher than 20 °C, the situation is exactly the other way round. The depth of the depth gauge will expand and decrease the measured depth.

Figure 29 shows the thermal induced mistake of the depth caliper. A caliper gauge measures the length at all used temperatures. Therefore he is stored thermally isolated at room temperature of about 20 °C and comes into contact with other temperatures only for the measurement. It can be assumed that he has the same temperature in all measurements in the core. In addition, the figure shows a linear expansion behaviour, which confirms this assumption. The errors are given as an extension in millimeters per meter length of the depth caliper at the different temperatures and each referenced to 20 °C.

As it can be seen, the maximum error at +60 °C is 0,4mm/m, or at -30 °C -0.4mm/m. The measured deflections of the pipes are less than one meter and 0,4 mm/m to measure is very low. This error should be neglected in the measurements. At a maximum measuring range of 300 mm of the depth caliper, the error at +60 ° C is exactly$0{,}363\ \mathrm{mm/m} \cdot 0{,}3\ \mathrm{m} = 0{,}109\ \mathrm{mm}$.

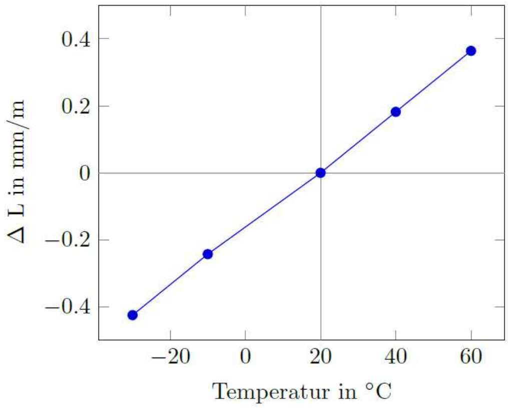

Figure 29: Thermal expansion of the depth caliper in the used temperature range

7.3.5 Time recording

In order to measure the creep behaviour properly and graphically, it is important to be able to stop the measurement period correctly. Since in the first hour the increase of the deflection increases the most, especially in this, the measuring duration must be exactly detectable. For each measurement, the exact time becomes recorded in the format hour:minute:second and the data processing program Excel calculates a time t_i, which elapsed between hooking in the test weight and measurement. Thus, the deflection should be recorded with time in seconds. The following clock is used:

Figure 30: Clock to measure the time period

A section of the test protocol describes the time recording more detailed.

1. Vorgang: Aufnahme der Referenzbedingungen unmittelbar vor Einhängen des Prüfgewichtes			
Uhrzeit:	h_1:	w_1:	t_1:
08 : 26 : 15	11,8 cm	0,00 cm	0 s
Notizen:			
2. Vorgang: Messung unmittelbar nach Einhängen des Prüfgewichtes			
Uhrzeit:	h_2:	w_2:	t_2:
08 : 26 : 30	13,44 cm	1,64 cm	15 s
Notizen:			
3. Vorgang: Messung nach Zeit t_3			
Uhrzeit:	h_3:	w_3:	t_3:
08 : 33 : 40	13,76 cm	1,96 cm	445 s
Notizen:			

Figure 31: Section of the test protocol

7.4 Test procedure

The test procedure consists of 10 measurements that are being carried out throughout the day. The procedure is as follows:

1. Setting the adjustment profiles to the required clamping length, 1.5 meters for single pipes and three meters for CoolFit pipes.
2. Setting the test weights
3. Storage the test pipes in the climatic chamber running overnight for temperature control to the target temperature
4. Positioning of the clock for time recording
5. Mounting the test pipe number one
6. Measuring the deflection due to its own weight and fixing the adjusting screw, so that the length cannot change due to friction on the bridge when pulling out.
7. Noting the deflection, opening the set screw and positioning the depth caliper for quick accessibility.
8. Hooking in the test weight and simultaneous reading of the second-precise time
9. Measuring the weight-loaded deflection and simultaneous reading of the second-precise time
10. Noting the time when the weight was hooked in, in procedure 1 (protocol), noting the time and the measured deflection in process 2 (protocol)
11. Mounting test pipe number two, three, etc. and repeat steps 5-10 until all test pipes are mounted and recorded by measurement.
12. After the last test pipe has been hooked in, re-record the deflection on all pipes after about five minutes.
13. After another 15 minutes, re-detect the deflection
14. Distribute the outstanding measurements to time intervals of the approximately equal period, so that the last measurement, number 10, occurs after approximately eight or nine hours.
15. After eight hours of measurement, unhook the test weights and label the test pipes with exact dimensions and test temperature (each pipe is only used for one temperature due to permanent deformation)
16. Storage of new specimens in climatic chamber and restart at point number 1.

7.5 Analysis

The deflection is recorded for the test and the modulus of elasticity is determined in the evaluation. This calculation is shown as an example in the following calculation. For this purpose, the first measuring point from Table A.4-1, in the appendix on page 76 of the German version, is used. Therefore is PB-H at -30 °C used.
The reference altitude at 08:41:00 is 12,52 cm. At 08:41:15 the height h_2 is 14,93 cm. For this measurement the test weight is hooked in. By comparing both times, it is noticeable that the time t_2 is 15 s. From this, the required deflection for calculating the modulus of elasticity can be calculated as follows:

$$\epsilon_2 = h_2 - h_1 = 14{,}93\ \text{cm} - 12{,}52\ \text{cm} = 2{,}41\ \text{cm} = 24{,}1\ \text{mm} \tag{7-4}$$

The modulus of elasticity is calculated by equation (A.39) of the appendix as follows:

$$\epsilon_i = \frac{F \cdot l^3}{48 \cdot E \cdot I} \rightarrow E = \frac{F \cdot l^3}{48 \cdot \epsilon_i \cdot I} \tag{7-5}$$

Therein, the test weight and the pipe dimensions for determining the area moment of inertia must be known. The test weight is measured on a scale with a maximum measuring range of $30\ \text{kg} \pm 1\ \text{g}$ to 2,67 kg and the dimensions with a Vernier caliper to d32,2x3,2 determined.
From these findings, the area moment of inertia can be calculated as follows:

$$I = \frac{\pi}{64} \cdot (R^4 - r^4) \tag{7-6}$$

With R for outer- and r for inner diameter:

$$I = \frac{\pi}{64} \cdot [R^4 - (R - 2 \cdot wst)^4] = \frac{\pi}{64} \cdot [(32{,}2\ \text{mm})^4 - (32{,}2\ \text{mm} - 2 \cdot 3{,}2\ \text{mm})] \\ = 31.021\ \text{mm}^4 \tag{7-7}$$

Finally, equation (7-5) can be calculated:

$$E = \frac{m \cdot g \cdot l^3}{48 \cdot \epsilon_1 \cdot I} = \frac{2{,}67\ \text{kg} \cdot 9{,}81 \frac{\text{m}}{\text{s}^2} \cdot (1500\ \text{mm})^3}{48 \cdot 24{,}1\ \text{mm} \cdot 31.021\ \text{mm}^4} = 2463 \frac{\text{N}}{\text{mm}^2} \tag{7-8}$$

The E-Modul for PB-H at -30 °C after 15 s is calculated to 2463 N/mm².

7.6 Results

7.6.1 Single pipes

The following diagrams show the e-modulus calculated in chapter Analysis7.5. All associated measured values can be found in the appendix, chapter A.4 from page 72 of the German version.
All figures are shown with the modulus of elasticity on the y-axis and the logarithmic loading time in seconds on the x-axis. The calculated measured values are shown with a marker. The solid line forms a resulting, logarithmic balance line.

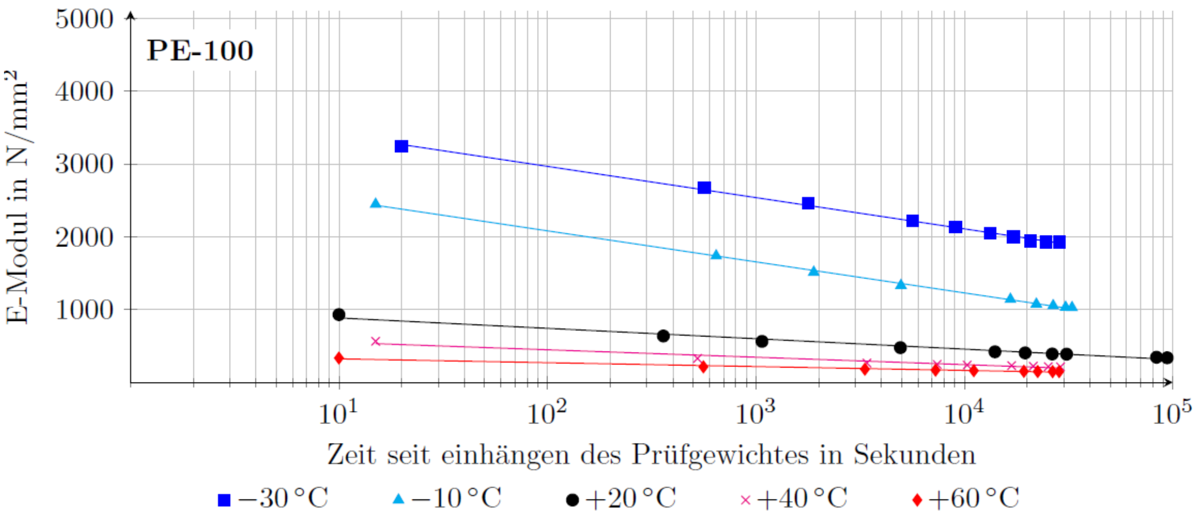

Figure 32: Results deflection behaviour PE-100 d32

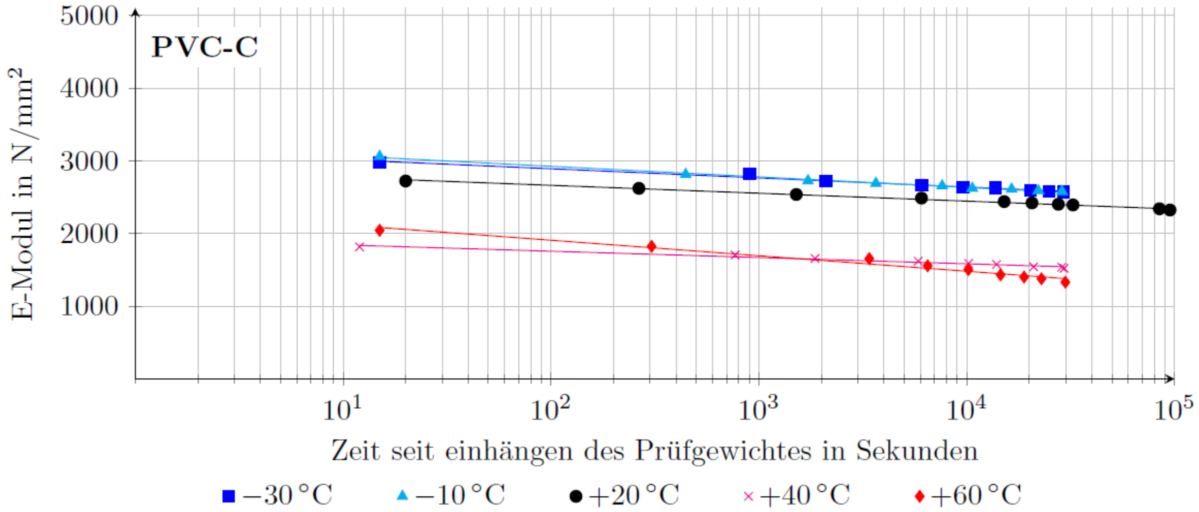

Figure 33: Results deflection behaviour PVC-C d32

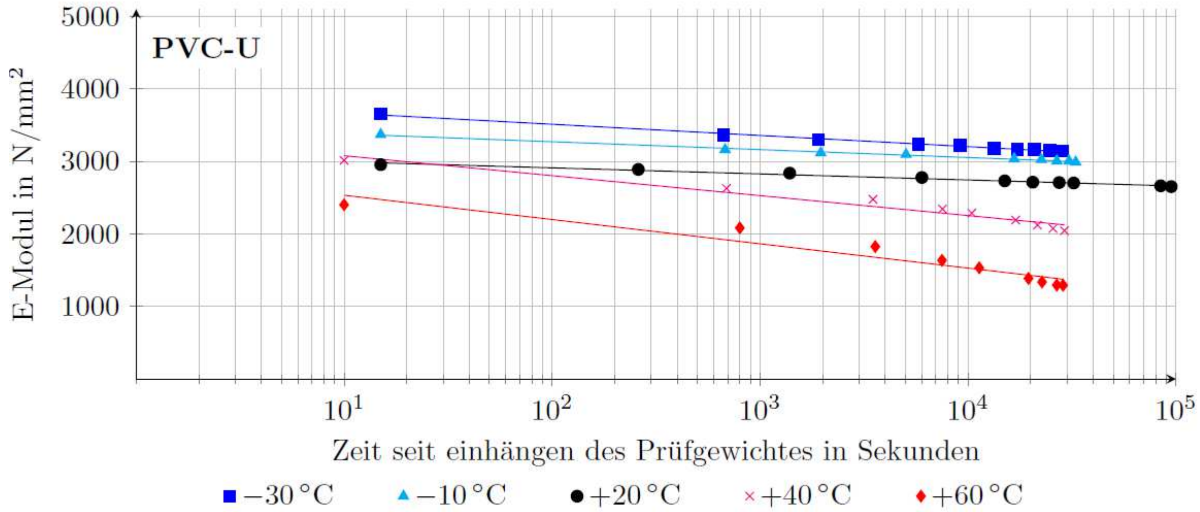

Figure 34: Results deflection behaviour PVC-U d32

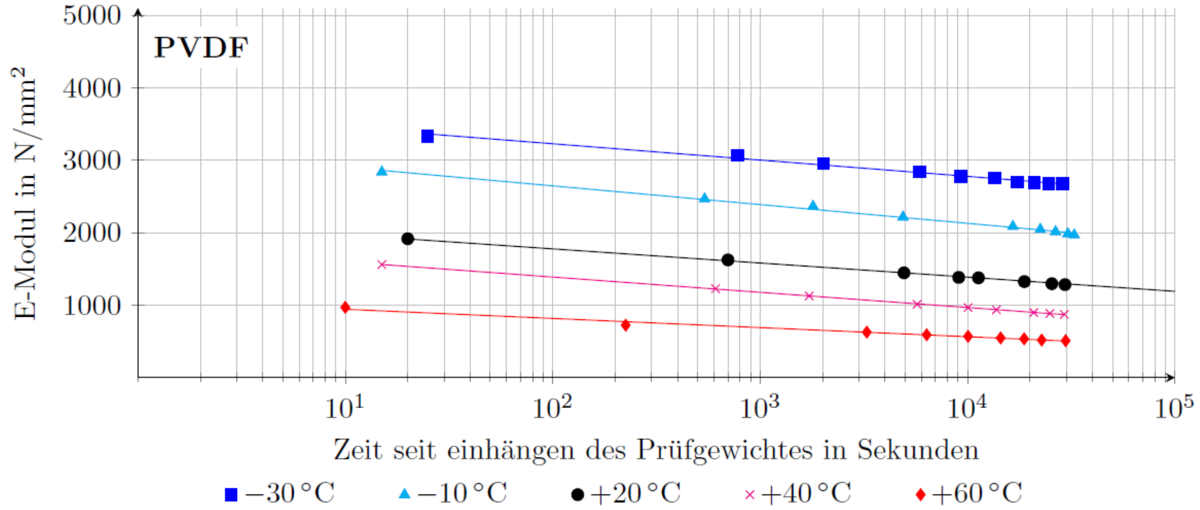

Figure 35: Results deflection behaviour PVDF d32

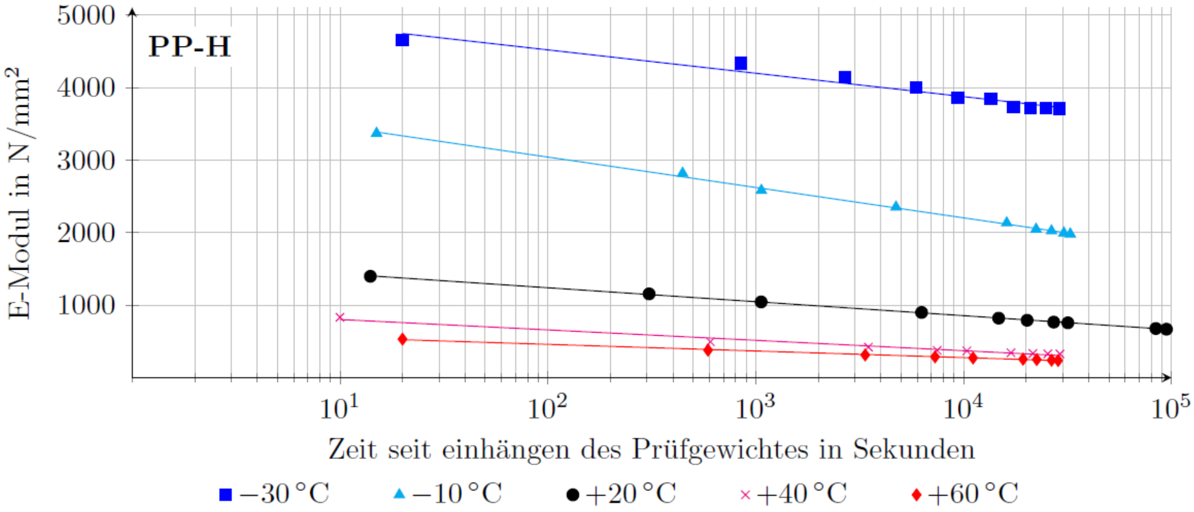

Figure 36: Results deflection behaviour PP-H d32

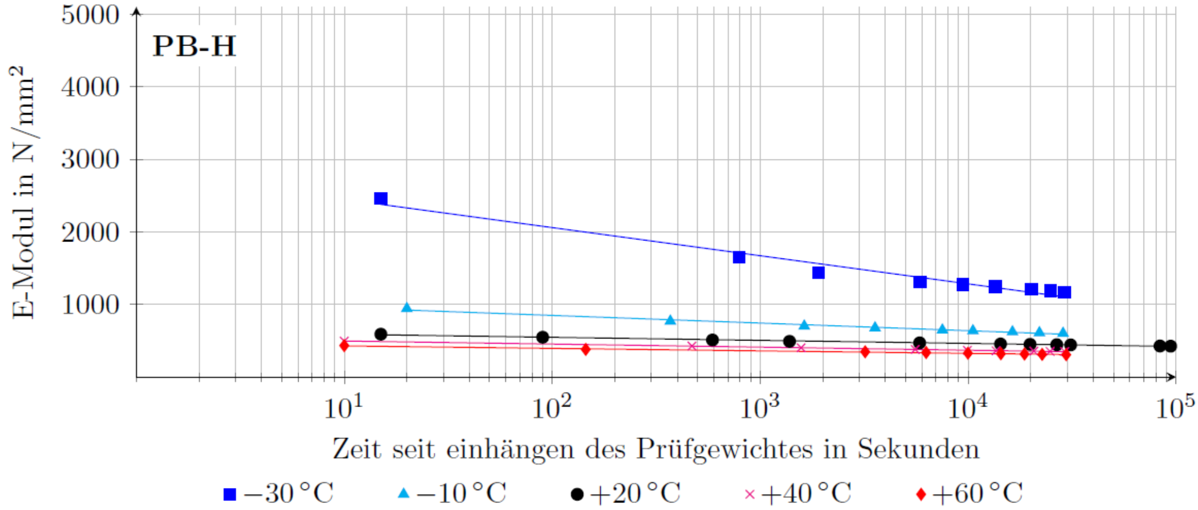

Figure 37: Results deflection behaviour PB-H d32

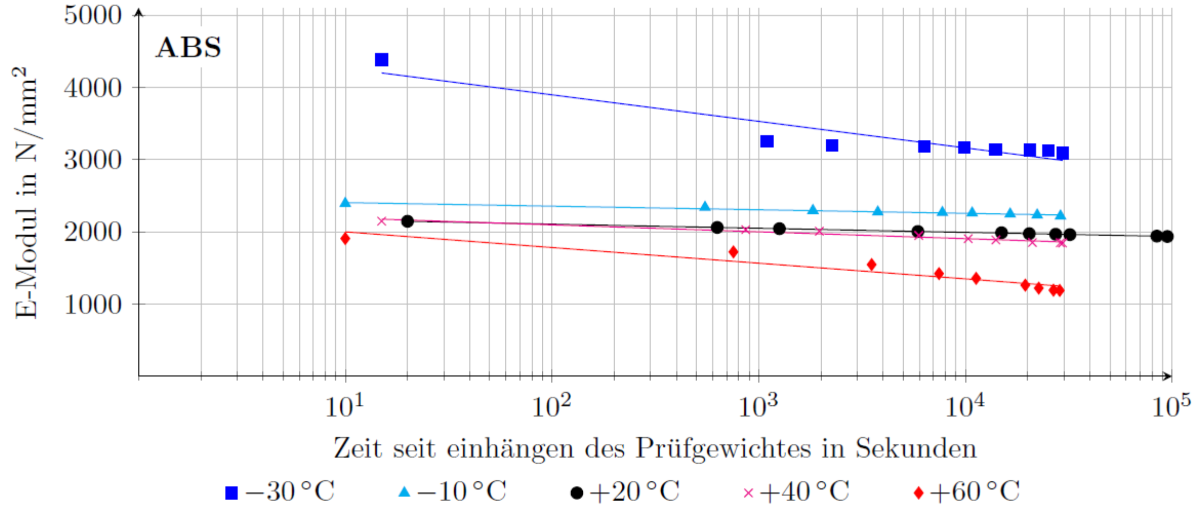

Figure 38: Results deflection behaviour ABS d32

7.6.2 Reproducibility measurements

In order to be able to make a reliable statement about the correctness of the measured experiments, reproducibility experiments should be carried out at +40 °C. Here, the remaining pieces of the single pipes are tested at the same test temperature. These are two ABS, two PVC-U and two PB-H pipes. The comparison is intended to allow a first statement whether the pipes have a large dispersion. It should be noted that the remaining samples are prepared from the same five meter bar and the comparison pipe from another bar. In addition, for a reliable statement about the scattering far more samples of each other bar are necessary.

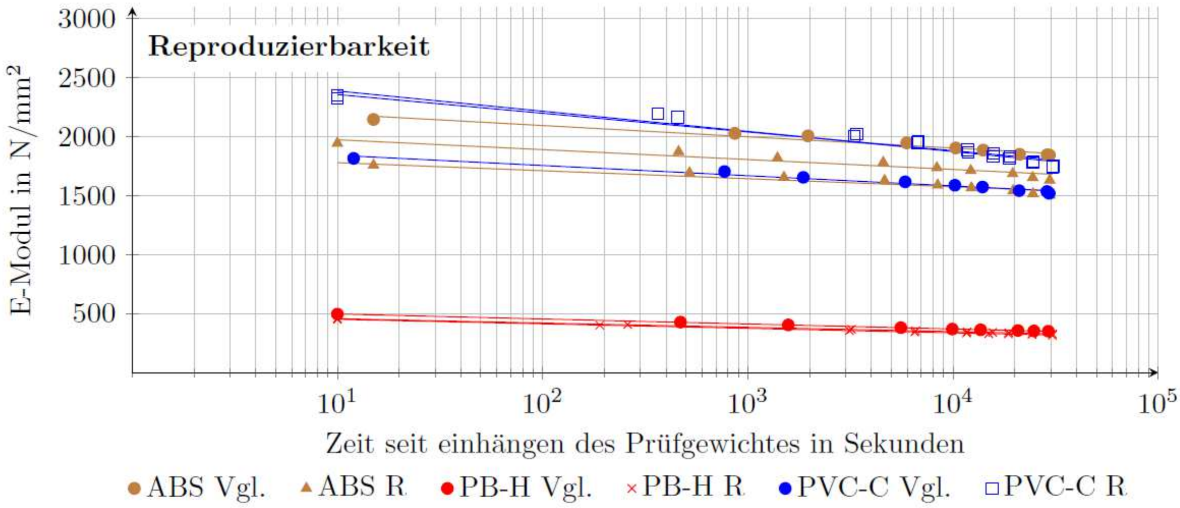

Figure 39: Results reproducibility experiments ABS, PB-H and PVC-C, d32

Figure 39 shows the results of reproducibility. There are one the one hand the so called “Vgl” test pipes and on the other hand “R” test pipes. The line of “Vgl” correspondents the line from the figures in chapter 7.6.1, the “R”-lines correspondents the reproducibility lines.
There are partly deviations between the comparison measurement (Vgl.) and the reproducibility measurement (R). The calculated values for PVC-C at +40 °C are too small at the beginning of the measurement and make no sense compared to the results of +60 °C. On the other hand, the results of the two test pieces in the reproducibility for PVC-C are the same. The calculated E-modules are also much closer to expectations. Nevertheless, it is clear from this examination that a great deal of diversification is possible.
Similar behaviour is also apparent in ABS. The two test pipes are at most 400 N/mm² lower than those of the comparison measurement. The results of both candidates also differ by < 200 N/mm².
The result of PB-H differs a little bit. Both comparison and reproducibility measurements are almost completely coincide.

7.6.3 Evaluation of single pipes

PE-100 is compared with the values of the literature vicarious for all test pipes. The values are compared with PE-100 by a densitiy of 0,95 g/cm³.In the literature, Figure 40: Literatur of the bending e-modulus for PE-100 [11, p.140 f], at 23 °C, after one hour, a bending creep modulus of 650 N/mm² is given. 400 N/mm² for +40 °C and equal duration. As can be seen, the values in the literature are larger than the calculated. They are for +20 °C 520 N/mm² and 290 N/mm² for +40 °C. One reason for this is that the test method in the literature according to standard, mainly with the three-point method. The method differs significantly from the deflection test carried out in this report. The three-point method uses a flat sample and not a pipe.

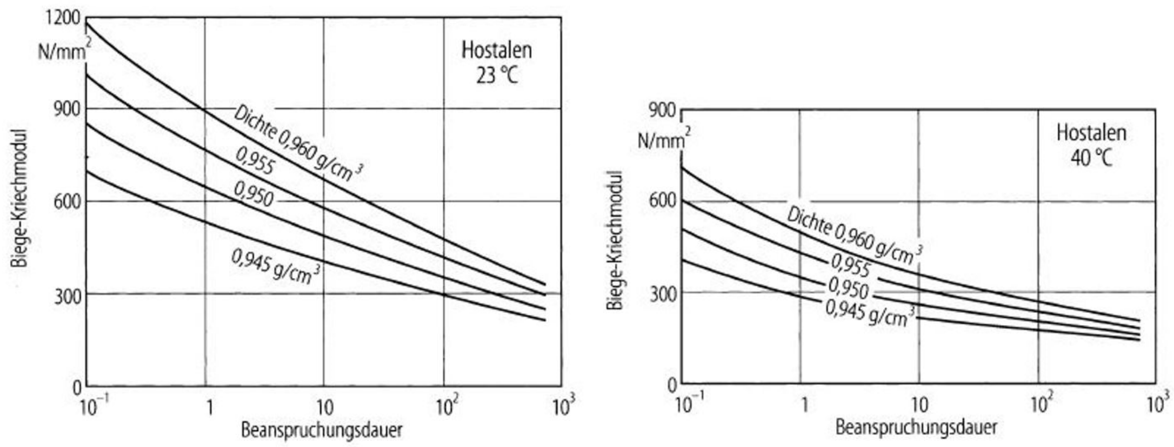

Figure 40: Literatur of the bending e-modulus for PE-100 [11, p.140 f]

Furthermore, in chapter 7.6.2 a reproducibility measurement on other plastic pipes shows a variance, which is larger than the deviation found in the literature. For comparison with PE, it can be concluded that a bending creep module can be calculated with the applied measuring method. In order to be able to determine a tolerance range of the measurement, it is necessary to carry out more reproducibility measurements for all temperatures, not just for one representative, and to make a statement about the compatibility of the literature with the determined scatter band. Due to the deviations found in the reproducibility measurements, the comparison is within a possible tolerance.

The figures from chapter 7.6 show the decrease of the e-modules with increasing time or temperature. It can also be seen, for example, that PB-H pipes in the temperature range from -30 °C to +40 °C have almost the same stiffness properties. This can also be recognized for PVC. PVC-U has a calculated modulus of 3800 N/mm² for cold temperatures of -30 °C and 2500 N/mm² for +60 °C. PVC-C at cold temperatures ~3000 N/mm² and for hot approximately 2000 N/mm². The difference between the modulus of warm and cold temperature is within a range of 1000 N/mm². This is different for pipes such as PP-H. For cold temperatures they show large e-modulus of about 4600 N/mm² and for warm temperatures only about 500 N/mm², respectively at the beginning of the measurement after about ten seconds. Similar behaviour can be observed for PVDF and PE-100.

In part, the effects of the determined reproducibility in the calculated modulus of elasticity are also shown. PVC-C is considered between +40 °C and +60 °C. At the beginning of the +60 °C has a larger modulus of elasticity than+40 °C. The same can be observed for PP-H between -10 °C and -30 °C or PVC-U between +20 °C and +40 °C.

In summary, the behaviour with regard to the stiffness properties can be assessed. PVC, PB-H and ABS pipes show temperature ranges in which their properties barely change. PE-100, PVDF and PP-H show big differences between hot and cold temperatures. Also the decrease of the modulus of elasticity with increase of the temperature can be observed well.
In order to be able to make a statement about the correctness of the calculated measured values, more reproducibility measurements are necessary. However, the calculated values give a first indication of the order of magnitude of the modulus of elasticity at the respective temperature.

7.6.4 EcoFit pipes

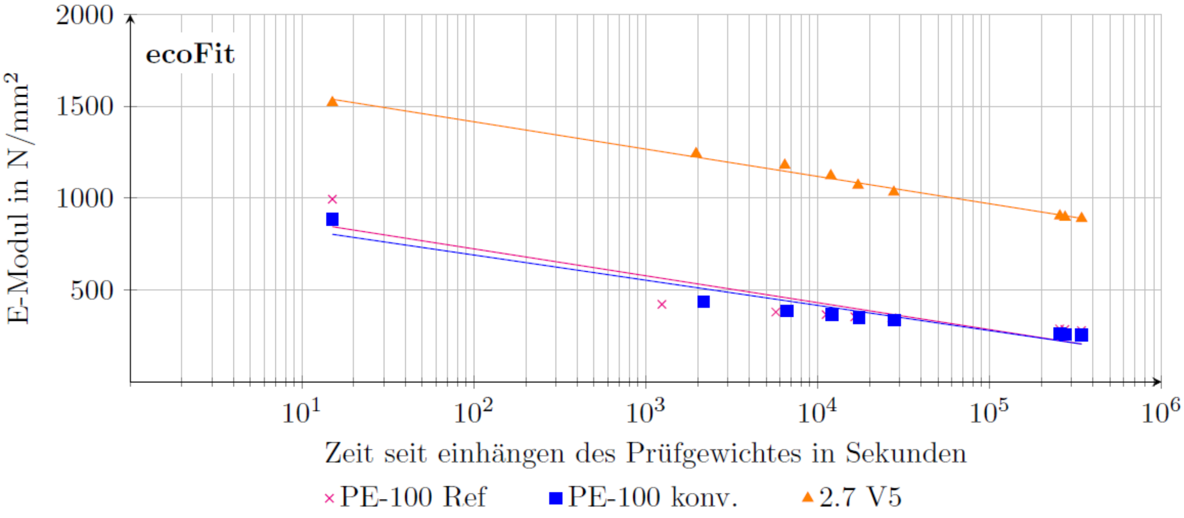

Figure 41: Results ecoFit for +20 °C

Looking at the figure, the higher modulus of 2.7 V5 is apparent. As expected, this is larger and can be attributed to the glass fiber-reinforced portion in the core. It is also noticeable that there is hardly any difference between the continuous three-meter-long PE-100 reference pipe and the pre-connected reference pipe, consisting of three one-meter-long, welded PE-100 pipe sections. The weld does not weaken the pipe.

7.6.5 CoolFit pipes

The evaluation of the CoolFit pipes differs slightly from the evaluation with ecoFit or single pipes due to the interaction of several layers. The procedure here is shown in the appendix on page 86 of the German version. On the y-axis the modulus of elasticity of the media-carrying inner pipe is applied.

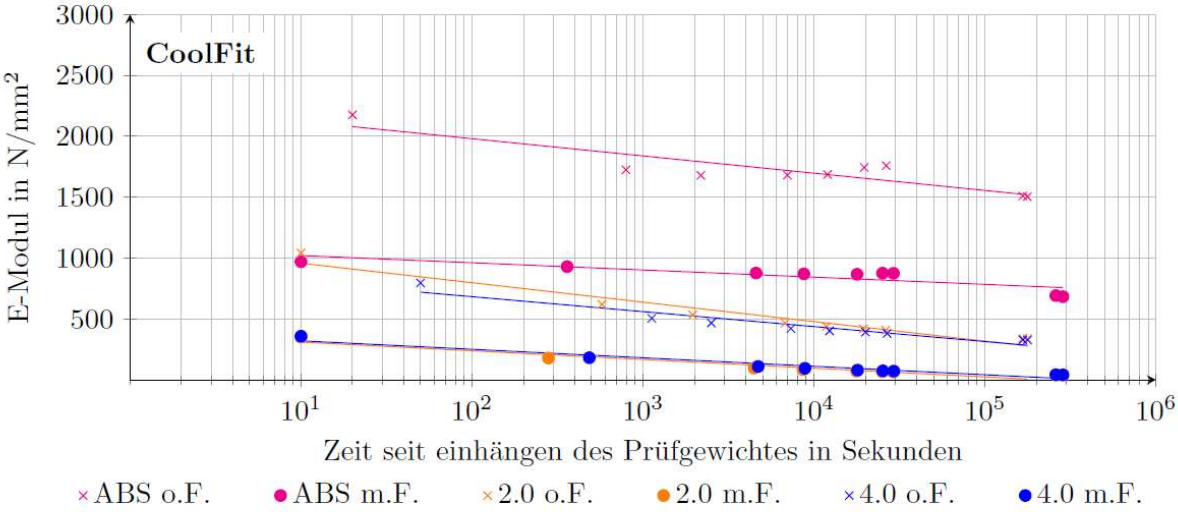

Figure 42: Results CF pipes with and without central welded fitting

There are significantly higher e-modules for CF ABS calculated compared to CF 2.0 and 4.0. Reason is that it is calculated back to the inner pipe and ABS, as already seen in chapter 7.6.1, has higher E-modules. Furthermore, it can be seen that the central fitting is a weak point. The modulus of elasticity drops by about half for all test pipes. That corresponds to the expectations. As a countermeasure, installation instructions are given by +GF+, according to which it must be avoided to install the connection point in heavily loaded areas. In general, they should be laid close to clamps, so that the bending moment in the fitting approaches to zero and that it is not subjected to any load.

The calculated e-modulus for CF 2.0 and 4.0 are almost completely identical. Due to the fact that the inner pipes are both made of PE-100, the results correspond with the expectations. Compared to chapter 7.6.1, almost the same moduli at +20 °C as for the load of the single pipe PE-100 dimension d32. This is about 950 N/mm² for the single pipe after ten seconds, and just under 1000 N/mm² for the same load time for CF 2.0 and 4.0. Also for CF ABS the match is ensured in the direct comparison. After twelve seconds, the modulus of elasticity of the single pipe as well as the CF ABS pipe is just 2100 N/mm².

The results of the calculation are satisfactory. The mathematical agreement with the single pipes, as well as the internal comparison between CF 2.0 and 4.0 shows a great security in the measurement process. The different approaches to evaluation provide the same insight. Only the creep behaviour is different. This is evident from the following chapter.

7.6.6 Creep resistance

For the comparison between the pipes, the creep resistance from equation (7-2) of all pipes shall be calculated. This requires a measurement duration of 1000 hours with E_{c3}, but the maximum duration are only ten hours. The creep resistance will be new defined because of this. The determined, logarithmic balance line is valid for a period of ten seconds to ten hours. The equation (7-2) is redefined as follows:

$$c_{c,DB} = \frac{E_{c3}(t = 10^1\ h)}{E_{c0}\ (t = 10^{-1}\ h)} \tag{7-9}$$

This results in the following figure for single pipes. The calculation can be seen in the appendix from page 87 of the german version.

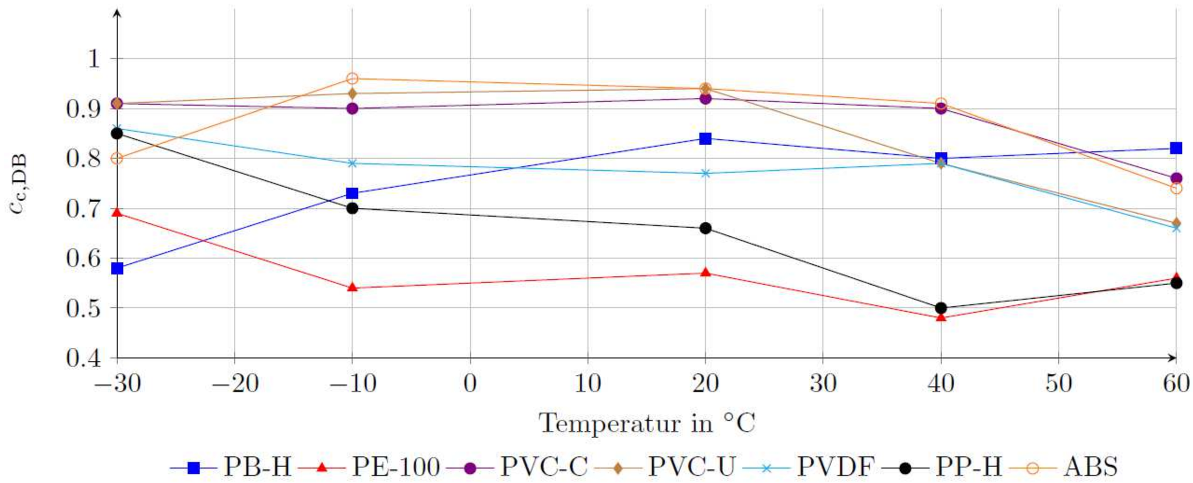

Figure 43: Results of the creep resistance for single pipes

Figure 43 shows how the creep resistance varies with the temperature of the individual pipes. There are three different types of behaviour. First of all, almost constant, as second increasing and as third one decreasing creep behaviour by increasing temperature.
A comparison between the values at -30 °C with those from +60 °C shows a tendency to decrease with increasing temperature. PB-H is the exception. For this candidate, the coefficient increases from 0,58 at -30 °C to 0,82 at +60 °C, an increase of 41,3 %.
Some candidates shows nearly the same behaviour at different temperatures. PVC-C and PVC-U barely differ in their behaviour between -30 °C and +20 °C. For this temperature range, both specimens

have the same creep strengths. PVC-C also for +40 °C. At this temperature PVC-U already drops from 0,9 at +20 °C to a value of 0,8. PVDF has also a constant creep behaviour in a temperature range from -30 °C to +40 °C with a value of approximately 0,8 per temperature be determined.
The maximum value of all measurements has ABS at a temperature of -10 °C. The creep resistance at this temperature is calculated to 0,96.

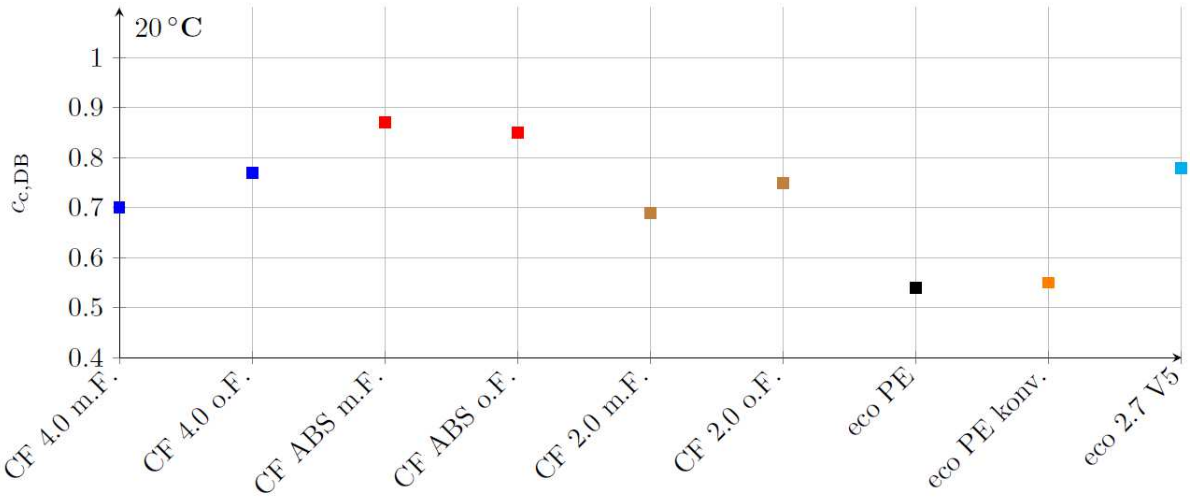

Figure 44: Results creep resistance CoolFit and ecoFit for +20 °C

The creep resistance of CF 2.0 and 4.0 with and without fitting, hardly differ. The reason is that the modulus of elasticity calculated back to the inner pipe, which is for both samples the same material. The creep resistance of CF ABS is higher than that of CF 2.0 and CF 4.0. A direct comparison with +20 °C shows that the bending creep resistance of the tested ABS single pipe is minimally greater than that of CF AB. Reverse behaviour is evident when comparing PE-100 with CF 2.0 and CF 4.0. Here, the creep resistance of CF pipes is slightly higher than that of the single pipe. The different creep behaviour of the CF pipes can be explained due the different own weight. The impact of the own weight isn´t considered in this work.
The continuous and pre-fabricated ecoFit PE-100 reference pipe does not differ in its calculated values. Their results have the same course of the modulus of elasticity and due this the same creep resistance. The calculated modulus of elasticity from the ecoFit PE-100 pipe coincides with that of the single PE-100 pipe. By comparing the creep resistance directly, no difference can be detected between them, which is satisfactory for the result of the measurement.
The 30 wt.-% glass fiber reinforced pipe shows, as expected, a higher creep resistance. This lies with a value of approximately 0,8 by 45 % over that of the reference pipe.

8 Solar impact

8.1 Test mode

A test stand shell be designed, which makes it possible to map the expansion behaviour of the test pipes due to partial heating of the surface temperature by simulation of the solar radiation. For this purpose, the pipe should be radiated on one side by a suitable radiation source (Caption 8.3.2). This test will be carried out in two different ways:

- There flows a medium through the pipes
- There flows no medium through the pipes

Due to the one-sided irradiation and the resulting, different surface temperature around the circumference, it is expected that the test pipe extent in the direction of the hot side. The test examines how the test pipe expands and whether it completely returns back to the original shape.
A customer note indicates that the surface temperature of pipes stored outside in summer months can increase to ~ +60 °C. For this reason, a radiation source in preliminary experiments, a distance and the associated radiation angle is determined to evenly establish a maximum surface temperature of approximately +60 °C.

8.2 Thermal radiation

Radiation is energy in the form of electromagnetic waves and spread without the help of a medium. This is the reason why the radiant energy arriving on Earth comes from the Sun. The energy power from sun is ~ $3{,}8 \cdot 10^{23}$ kW . Or $63.500\ \mathrm{kW/m^2}$ converted to its surface. This huge energy results from a core merger from hydrogen to helium. In this process, energy is released in the form of radiation. [17, p.38]
Sun radiates in all directions, only a fraction of these hits the earth's surface. This is given with the irradiance “E” and is defined as the radiant energy δQ, which strike a surface δA per unit of time δt. This extra-terrestrial radiation was published by the World Meteorological Organization Genf, WMO for short, in the publication 590 of 1982 by $136{,}7 \pm 0{,}7\ \mathrm{mW/cm^2}$,which is the equivalent of $1367\ \mathrm{W/m^2}$.
There are different types of radiation with different energy content Figure depending on the wavelength λ. The following figure shows an overview of the classification of the different wavelengths.

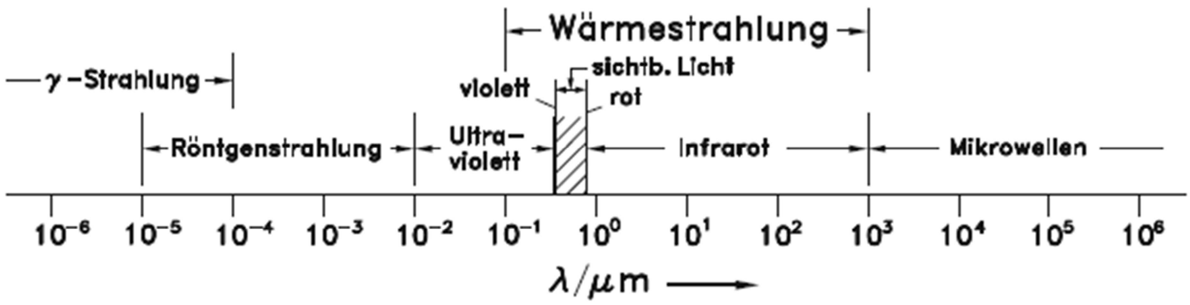

Figure 45: Spectrum of electromagnetic wavess

The middle range, with wavelengths between about 0,1 and 1000 µm, is called temperature or heat radiation. The visible light (0,38 µm to 0,78 µm), which the human eye can perceive, is located in this area. The wavelength interval $0{,}01\ \mu m \leq \lambda \leq 0{,}38\ \mu m$ is the range of ultraviolet radiation. Between $0{,}78\ \mu m \leq \lambda \leq 1000\ \mu m$ lies the infrared radiation. Each wavelength has its own frequency “f”, so the following relationship exists: $c = f \cdot \lambda$, where “f” is the Frequency and λ the wavelength. It follows that the frequency decreases with increasing wavelength. From this result, the long wavelength is particularly low and short wavelength very high in energy. Max Planck succeeded with his “ Planck's radiation law”. This law gives a relationship between the energy content of a black emitter electromagnetic energy and the wavelength.

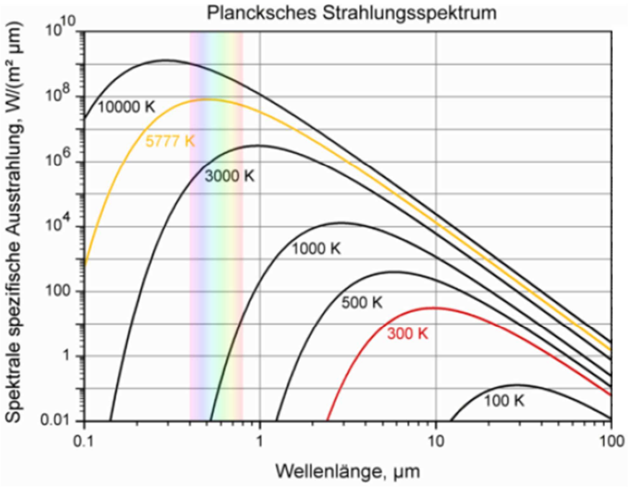

Figure 46: Energy content of electromagnetic energy from black emitters [20, p. 316]

Figure 46 shows the radiation intensity of black bodies as a function of their wavelength. λ_{max} is the wavelength at which the intensity reaches their maximum. The line with yellow color shows the spectral specific radiation of the sun. This comes close to the distribution of a blackbody with the surface temperature of 5777 K. The human eye perceives bodies with the color at which the maximum intensity is reached. According to the “Wien shift theorem”, which say that the product of maximum wavelength and surface temperature is constant, the perceived color of the sun can be calculated. T^* denotes the temperature of the blackbody: [21, p.5-1 ff]

$$2989\ \mu\mathrm{m} \cdot \mathrm{K} = \lambda_{\mathrm{max}} * \mathrm{T}^* \rightarrow \lambda_{\mathrm{max}} = \frac{2898\ \mu\mathrm{m} \cdot \mathrm{K}}{\mathrm{T}^*} = \frac{2898\ \mu\mathrm{m} \cdot \mathrm{K}}{5777\ \mathrm{K}} = 0{,}517\ \mathrm{K} \qquad (8\text{-}1)$$

The color is associated with this wavelength orange-yellow, which is why the human eye perceives the sun by this color. The higher the surface temperature of black emitters, the more they move into the ultraviolet or very short wavelength range and gain in energy content. [22, p.99]

8.3 Preliminary tests

Preliminary tests are carried out in which a sequence and various attitudes are examined, which are later of importance for the construction and execution of the main experiments. It is primarily a suitable radiation source for imaging the solar radiation. For this, a distance to the pipe, and a distance between two radiation sources is checked. In addition, different measuring methods for the temperature absorption of the surface are investigated and compared with each other. This helps to measure the correct surface temperature and not any other value.

8.3.1 Preliminary test construction

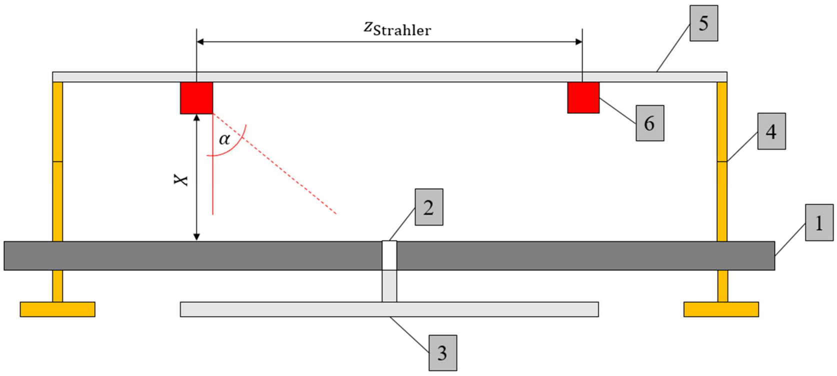

Figure 47: Construction for preliminary tests

The preliminary test stand consists of a test pipe {1}. A CF ABS d32 / D90 is used therefore. The pipe is fixed by a pipe clamp in the middle between both ends{2}. A small substructure protects the experimental setup from falling over {3}. The yellow color shows spotlight tripods {4}, which are connected by a Minitec-profile {5}. The examined spotlights {6} are fixed by two screws in this profile. The tripods can be adjusted in their height by a set screw. A distance of X=90 cm can be adjust easily. The distance “z” can be set along the length of the Minitec-profile.

8.3.2 Selection of a suitable radiation source

For the selection of a suitable radiation source {6} in Figure 47, various artificial light sources come into the selection. It´s compared how they´re similar to natural light, but also what heat radiation emanates from them.
For the artificial irradiation of plastics, the use of xenon arc lamps is recommended in the literature (Figure 48: Xenon arc lamps in their structure (Drawing from Osram AG) [22, p.104]). These have a homogeneous spectrum and are closest to that of natural sunlight. They´re used, for example, for cinema lighting or headlights in automobiles. However, the artificial irradiation according to DIN aims at the aging of the plastics, which shouldn´t be investigated in the test mode in chapter 8.1. Xenon arc lamps are expensive and therefore can´t be included in the selection

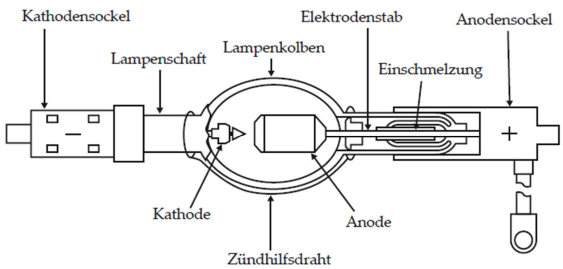

Figure 48: Xenon arc lamps in their structure (Drawing from Osram AG) [22, p.104]

In the case of artificial light sources, a distinction is made between thermal radiators, low-pressure discharge lamps, high-pressure discharge lamps and electroluminescent radiators.
The most common thermal radiators are light bulbs or halogen lamps. A tungsten wire coil is located in an evacuated or gas-filled glass bulb for a light bulb. For halogen incandescent lamps, the bulb consists primarily of quartz glass, because the tungsten wire coil heats up to higher operating temperatures. This also includes additions of halogen compounds. [23, p.79 ff.]
The most common low-pressure discharge lamps are fluorescent lamps or compact fluorescent lamps. The operating principle of discharge lamps is that the piston is filled with xenon or krypton gas and operated at a vapor pressure of about 10^{-6} to 10^{-7} bar. When switching on, electrons are released, which start a chain reaction. This emits radiation mainly in the invisible UV range. A layer on the inside of

the pipe absorbs this radiation and converts it partially to visible light. [23, p.96]
The following table shows the spectrums of different radiation sources and compares them with solar spectrum.

Table 18: Energy consumption of different light sources [24, p.228]

Type	Summary radiation	UV 250-380 nm in %	Visible 380-780 nm in %	IR-A 780-1400 nm in %	IR-B 1400-3000 nm in %	IR-C >3000 nm in %
Light bulbs	93	0,05	10	37	31	15
Halogen light bulbs	94…96	0,1…0,8	13…18	38-42	28…32	10…15
Fluorescent bulbs	65	0,5	20…30	1	0,2	35…45
Compact fluo-rescent bulbs	70	0,5	25…30	1	0,2	38…42
Global radiation	100	5	54	30	11	-

Table 18: Energy consumption of different light sources [24, p.228] shows the energy balance of different lamp groups divided to their according to proportions of the radiation flux in defined spectral ranges. The percentages refer to the absorbed power of the lamp. For the selecting of a suitable light source for the irradiation of the pipes, it should be compared, which lamps have a high heat production to reach +60 °C surface temperature and which one are the closest to the global radiation.
When considering the heat production, it is important to check the long wavelength components, which means to pay attention to the IR shares. Discharge lamps have the largest proportion of IR-C radiation, but there are no matches to the global radiation. Global radiation has no IR-C radiation. When looking at the IR-A component, the greatest agreement occurs in the case of both temperature radiators. In the case of halogen light bulbs, there is greater heat production. Light bulbs have a smaller deviation from the global radiation. In the visible portion, the discharge lamps are the most suitable. However, all light sources are still far from the yield of global radiation. It is also noticeable that due to the high IR-C content of discharge lamps, a significantly lower total radiation flux compared to global radiation is present than the case with halogen incandescent lamps. The decision of a suitable radiation source therefore falls on halogen light bulbs, as used for example in construction spotlights. They have the largest total radiation flux compared to the global radiation, as well as the largest heat production.

8.3.3 Distance of the radiation source

In several experiments and different distances “X” of the radiation source temperature curves, as shown in Figure 50 and Figure 51, were recorded. The resulting stationary temperatures, plotted over the distance X, result in the following figure. It consists of four measurements.

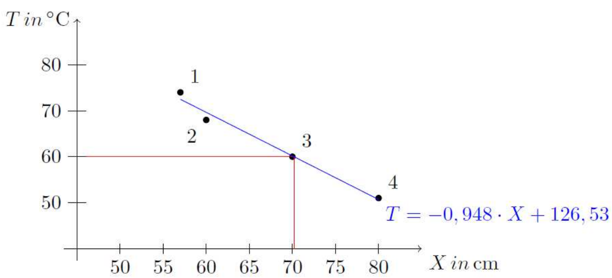

Figure 49: Stationary temperatures depending on distance "X"

Due the resulting line, the distance of the radiation source can be calculated:

$$T = -0,948 \cdot X + 126,53 \rightarrow X = \frac{T - 126,53}{-0,948} \tag{8-2}$$

T is in °C, the result is calculated to:

$$X = \frac{60 - 126,53}{-0,948} = 70,2\ \text{cm} \tag{8-3}$$

This results in a distance of approximately 70 cm. The resulting temperature profile, for the determined distance in the test pipe, is shown in Figure 50: Temperature recording for a distance X=70 cm. The following nomenclature must be observed. Each PT element in depth “s”, see also Figure 52 on page 47, with s = 83 mm, s = 75 mm or s = 68 mm is nomenclated as T_s. These temperatures are recorded for the calculation schema according to chapter 8.3.4.1. In addition, the surface element has the color red, which is shown in Figure 53 or as $T_{Oberfläche}$ in the legend. The ambient temperature is $T_{Umgebung}$.

The temperatures change after a period of 180 minutes, which corresponds to three hours, barely. Based on this finding, the minimum irradiation time of the main experiments is set at four hours. The drop in surface temperature after 90 minutes irradiation time is due to the contact measurement, according to chapter 8.3.4.2. The cold tip of the contact measurement is held on the insulation tape. Due this, the glued PT element is cooled. It reaches the original temperature a short time after the contact measurement is finished again. In addition, a sensitive behaviour of the surface PT elements can be observed. Bypassing air cools strongly. With this realization, windows and doors should remain closed for the main test, in order to keep these fluctuations as small as possible.
The slight increase in temperature after three hours of irradiation can be attributed to the ambient temperature. The start of the experiment for Figure 50 is at 09:42 o'clock. The ambient temperature at this time is 23,73 °C and gradually increases according to $T_{Oberfläche}$. At the end of the experiment at 12:51, the temperature is 25,42 °C and rising. Further measurements show this dependence.
Figure 51 is for a distance from 60 cm and was taken overnight, which explains the long test time of over 900 minutes. The measurement begins at 15:57 and ends at 08:22 of the following day. It clearly shows how the ambient temperature affects the individual temperatures. While it hardly changes the first 250 minutes, the temperature measuring points also show steady state behaviour. When the room temperature drops at around 8:30 pm, after 250 minutes, the temperatures drop successively, first on the surface then on the inside.

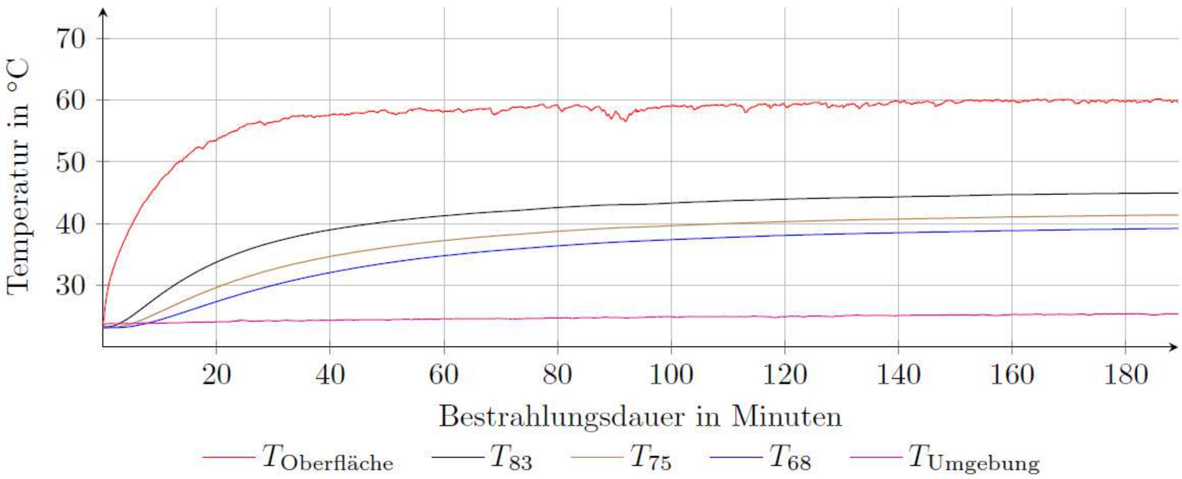

Figure 50: Temperature recording for a distance X=70 cm

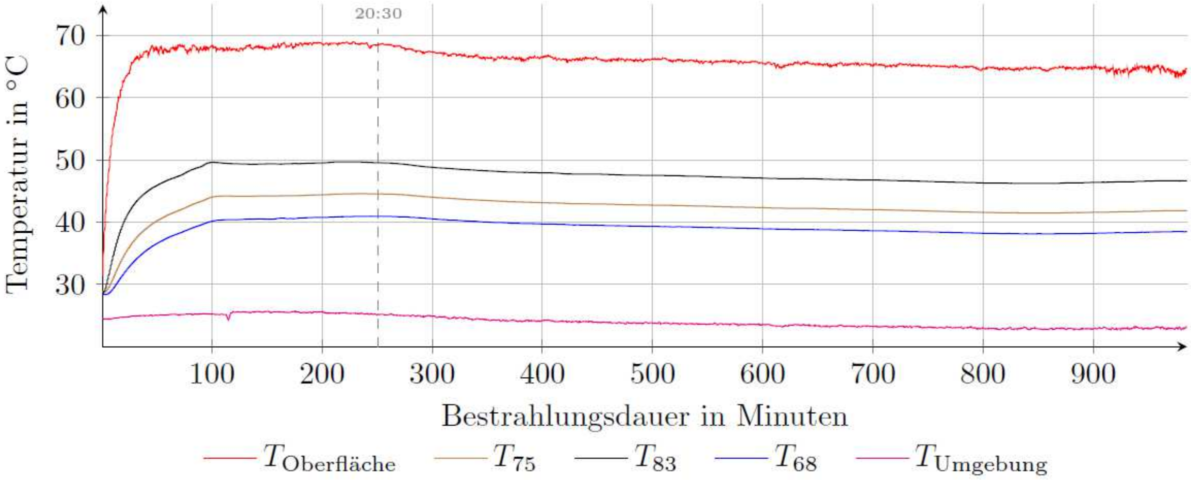

Figure 51: temperature recording for a distance X=60 cm

8.3.4 Temperature measurements

To measure a correct surface temperature when carrying out all main experiments, the installation of PT temperature sensors on the surface should be compared with alternative measuring instruments.
The following two measuring methods are used for a temperature measurement:

- Calculation schema
- Glued PT elements on the surface

In the calculation (Figure 52), the temperature is recorded at three different depths. This is necessary to measure the temperature profile through the pipe, because materials and their thermal conductivity coefficients are known. So the surface temperature can be calculated back.
This calculated value is compared with the measured temperature by a glued PT element by a black PE tape (Figure 53). If both values agree, it can be assumed that the measured temperature corresponds to the truth. If the two values do not agree, it is necessary to compare them with alternative measuring instruments and apply the method which gives more agreement to the main experiments. The following figures shows both methods:

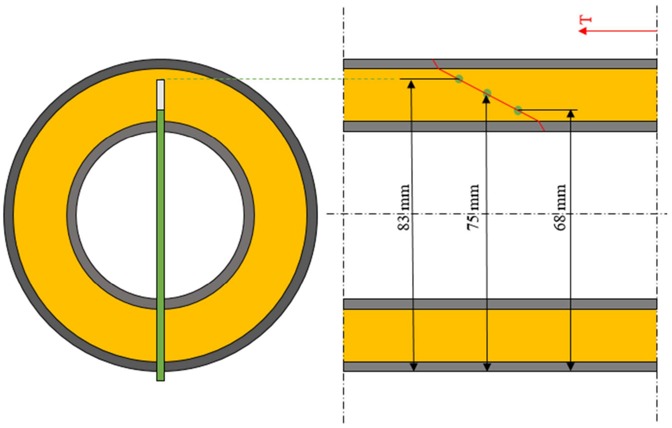

Figure 52: Claculation scheme

Figure 53: Glued PT-Element on the surface

8.3.4.1 Calculation procedure of the surface temperature

The calculation assumes that the temperature profile can be calculated by using the formulas of a multilayer board. The reason for this is that the heat flow hits the surface on one side and only from above. The calculation as a cylinder jacket is used when the heat flow is distributed around the circumference and hits from all directions by the same value on the profile.
First of all, the heat flow $\dot{Q}$ in the area of the insulation is calculated by the following formula:

$$\dot{Q} = \frac{\lambda_{Isolation}}{\Delta s} \cdot A \cdot \Delta T \qquad (8\text{-}4)$$

$$\dot{q} = \frac{\lambda_{Isolation}}{\Delta s} \cdot \Delta T \qquad (8\text{-}5)$$

The experiment showed that the PT elements do not detect the temperature with the tip. They measure with the entire range of their measuring tips, shown in white in Figure 52. That must be considered for “s”. In addition, temperature sensor T_{68} is consequently excluded from the calculation because not the whole part of the area is in the insolation and therefore it is not possible to make a statement about the exact depth. Equation (8-5) is changed as follows:

$$\dot{q} = \frac{\lambda_{Isolation}}{s_{83} - s_{75}} \cdot \Delta T \qquad (8\text{-}6)$$

Due the length $l_{Messbereich}$ of the measuring area follows:

$$s_{83} = 83\,mm - \frac{l_{Messbereich}}{2} \qquad s_{75} = 75\,mm - \frac{l_{Messbereich}}{2} \tag{8-7}$$

By using the radius does this mean:

$$r_{83} = s_{83} - \frac{D}{2} \qquad r_{75} = s_{75} - \frac{D}{2} \tag{8-8}$$

Equation (8-6) has changed to:

$$\dot{q} = \frac{\lambda_{Isolation}}{r_{83} - r_{75}} \cdot \Delta T \tag{8-9}$$

Right now it is possible to calculate $\dot{q}$. Due this the temperature on the inner side of the PE pipe can be calculated:

$$T_{PE-innen} = \frac{\dot{q}}{\lambda_{Isolation}} \cdot (r_{PE-innen} - r_{83}) + T_{83} \tag{8-10}$$

Finally, it is possible to calculate the surface temperature:

$$T_{PE-außen} = \frac{\dot{q}}{\lambda_{PE}} \cdot (r_{PE-außen} - r_{PE-innen}) + T_{PE-innen} \tag{8-11}$$

The following table shows the calculated values. They correspondent to the stationary values for X=70 cm.

Table 19: Calculated values of the surface temperature for X=70 cm

$\lambda_{Isolation}$	λ_{PE}	$l_{Messbereich}$	D	T_{83}	T_{75}	$\dot{q}$	$T_{PE-außen}$
$0{,}022\,\frac{W}{m \cdot K}$	$0{,}38\,\frac{W}{m \cdot K}$	14 mm	75 mm	45,26 °C	40,93 °C	$11{,}908\,\frac{W}{m^2}$	52,838 °C

8.3.4.2 Comparison with alternative measuring instruments

The calculation schema yields a surface temperature of 52,838 °C. The glued-PT element as shown in Figure 53 measured a temperature of just under 60 °C for a distance “X” of 70 cm. These values differ significantly. The calculated value according to the calculation scheme is just under 7 K below the measured value, so only one of the two methods can be used for the main experiments. The comparison with alternative measuring instruments should bring a decision which method is used.
The following measuring instruments are used to compare the values:

- Contact measuring by a test bulb
- Contactless measurement with infrared measuring device
- Contactless measurement with thermal camera

The following table shows the results of the comparing measuring instruments for a distance of X=70 cm and a emission coefficient of ϵ=0,95.

Table 20: Results of the comparitive measuring instruments for X=70 cm

Nr.	Measuring instrument	$T_{Oberfläche}$	Notice
1	Glued PT-Element	59,63 °C	Accordance to Nr. 3,4 and 5
2	Calculation schema	52,838 °C	No accordance
3	Contact measuring	57,7 °C	-
4	Infrared measuring	60,6 °C	-
5	Thermal camera	60,17 °C	-

The glued PT element complies with the infrared and thermal camera measurements. The difference to the contact probe is just under two Kelvin. The calculation schema does not show any significant matches with differences greater than 4,9 K.
The glued PT element brings more agreement to independent measuring instruments. Because of this, this method should be used for surface measurement. The calculation scheme also has the disadvantage that it is very complicated and the exact depth, at which the temperature is detected, is difficult to determine and manufacture. In addition, when preheating the contact probe, the difference to the glued PT element is significantly lower. The black PE adhesive tape makes it possible to assume that the sensor heats up to the same temperature as the black pipe surface. In addition, it is a very simple method, which makes it possible to record a temperature profile over the irradiation period. Images of the thermal camera and infrared recordings are performed comparatively.

8.3.5 Radiation angle

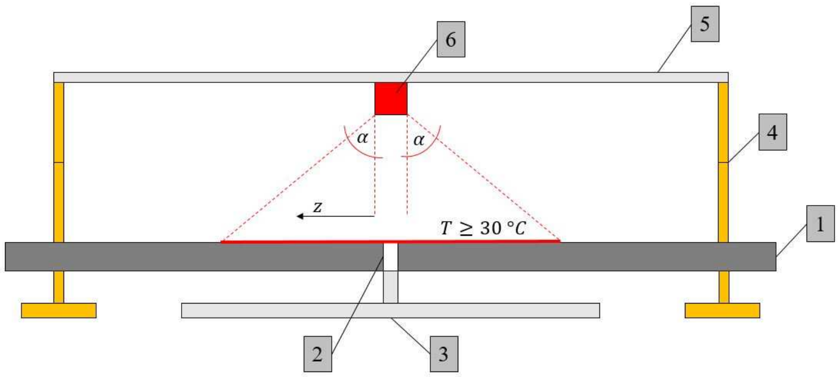

Figure 54: Construction to determine the radiation angle of the source

In order to be able to determine a distance between two radiation sources in the “z” direction, the radiation angle is finally examined. The test stand to examine this is shown in Figure 54.
To simplified the measurement, it is assumed that every site of the spotlights {6}has the same radiation angle. It should also be noted that the end of the irradiated area begins as soon as the measured surface temperature falls below 30 °C.
The experiment should be done for X=70 cm. The surface temperature is measured at a distance of 3 cm with the contact measurement. It is measured by the contact probe, because it is the easiest way and it handles and records the temperature at the right place. In addition, the measured values are served as a guide. If the radiation angle is detected and two radiators are connected parallel by the discovered distance “z”, images of the thermal camera should illustrate the course of the temperature in the irradiated area and shows possible corrections.
For the illustrated experimental setup, the following temperature profile results.

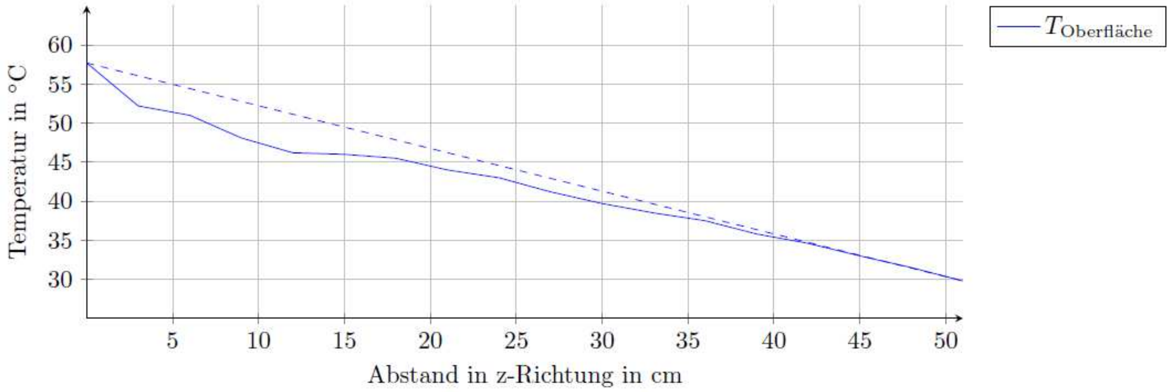

Figure 55: Temperature recording in z-direction by a distance X of 70 cm

At a distance of approximately 53 cm, the measured temperature falls below 30 °C. The resulting angle is calculated to $\alpha = 36°$. The measured values and the calculation are shown in the appendix on page 89 of the German version. The distance z_{Strahler} is calculated to 58 cm. Further experiments and recordings with a thermal camera show that due to the radiation superposition of two neighboring radiation sources 72 cm must be kept. The following taken image with thermal camera shows the temperature distribution on the pipe surface between two radiation sources for X=70 cm and z=72 cm.

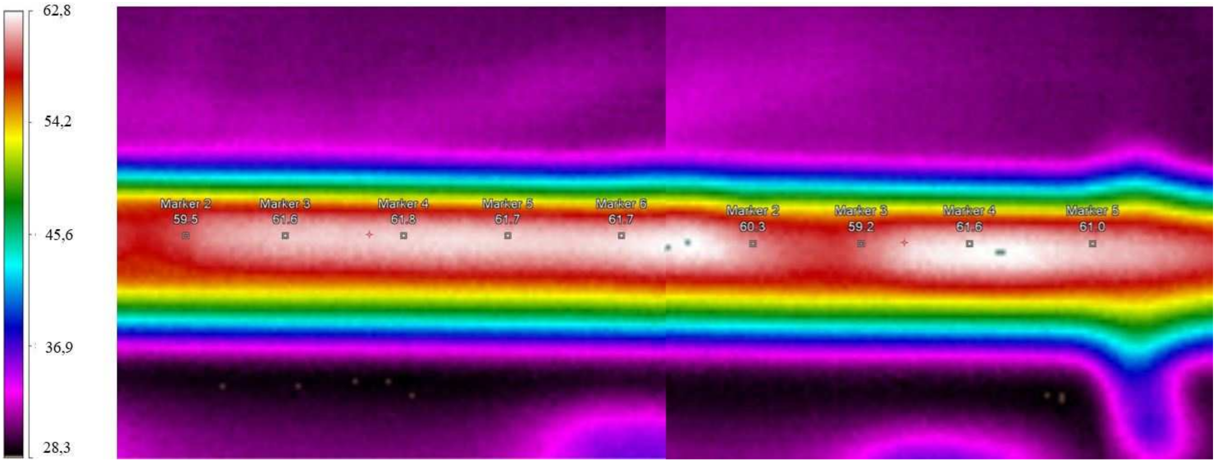

Figure 56: Temperature on the surface taken by a thermal camera for X=70 cm and z=72 cm

8.3.6 Summary of the preliminary tests

For the main experiments, temperature measurements are carried out according to the glued PT element. Based on the results of preliminary tests, the following summary is agreed with +GF+:

1. Temperature measuring:

   Two direct-irradiation temperature measuring points, two to indirect radiation, one is at the direct Irradiation at 90°, one at 180° of circumference and one at the junction between insulation and inner pipe. The remainder of the PT sensor measures the ambient temperature. An overview as well as the nomenclature is shown in the Figure below.
2. Distance X: 70 cm
3. Distance z: 72 cm
4. $\Delta T_{max} = \pm 5$ K

   ΔT_{max} describes the maximum difference around the average of the surface temperature.

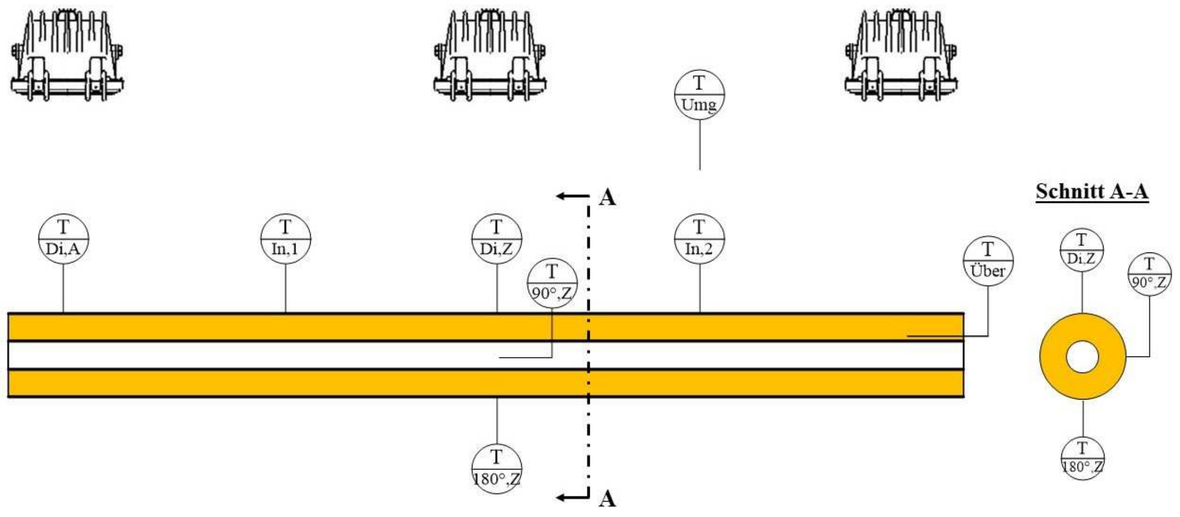

Figure 57: Temperature recording for the radiation of the pipes

8.4 Main tests

On the basis of the findings from preliminary tests, a test stand is designed which allows to observe the points described in the summary. The test stand is described in the following chapter.

8.4.1 Test construction

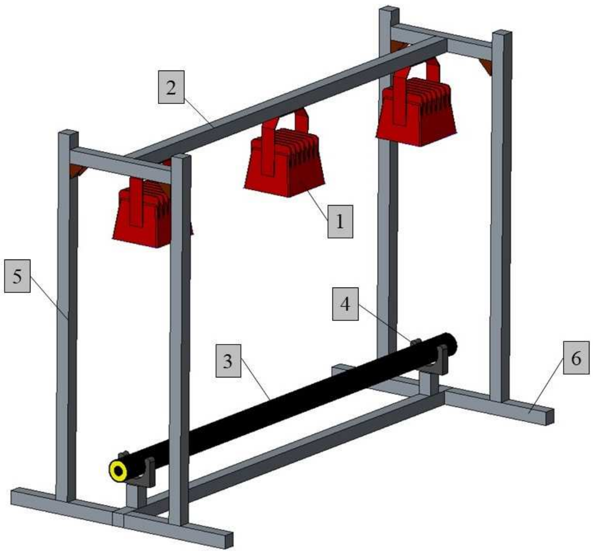

Figure 58: Main test stand for the solar radiation

The test stand simulates as far as possible the storage and installation outdoors. The selected halogen spotlight {1} are used to image the solar radiation and are screwed onto a common longitudinal profile {2}. Due this, the X-distance is identical for all radiation sources. The radiated test pipe {3} is held in a Clip-it clamps {4} by the correct dimension. These have a distance of 1,60 meters. This distance corresponds to the same as it is used in the practice. The radiated test pipe has a length of 1.80 meters. The experimental setup has four guide profiles {5}, which are used to set a distance X. In order not to fall over, these are screwed on feet {6}, which give the construction a stable state.
The test stand radiates the test pipes from one side for a long time while the pipes can´t rotate sideways. It simulates the one-sided distortion behaviour in one-sided irradiation. It is an extreme case and does not include shadows, gusts of wind or a changing sun position. In a further experiment, the behaviour in the installation is additionally examined by clamping a pipe of five meters in length and supporting it at both, free ends with supports.

8.4.2 Test procedure

The following test procedure is chosen:

1. Fixing the test pipe in the Clip-it clamps and set the distance X
2. Connect the glued PT-Elements
3. Start LabView to record the temperature profile
4. Mark the places to measure the height (maximum moving away)
5. Measuring the heights by switched off lightspots
6. Start the saving from LabView
7. Switch on the lightspots
8. Measuring the heights immediately after switching on the spotlights and every 15 minutes again due the first hour of irradiation
9. Until switching off the spotlights measuring of the heights every hour
10. If a stationary behaviour can be observed in LabVIEW (after about four hours) taking pictures by the thermal camera
11. Switching off the spotlights
12. Measuring the heights immediately after switching off the spotlights and every 15 minutes again
13. Stop saving data in LabView after every temperature is lower than 30 °C

8.4.3 Maximum warpage

Maximum warpage is a quantity size that should measure the maximum deviation from the initial shape. For this purpose, the pipe is compared with its zero position and as a result the maximum distortion is calculated. The following figure shows the expected result for one-sided irradiation. The pipe clips are shown on the left and right sides. These hold the pipe so that it can´t turn to the side.

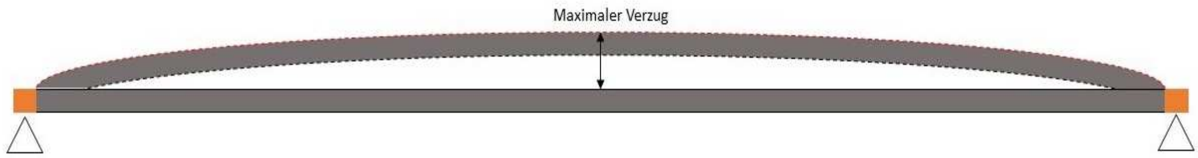

Figure 59: Maximum moving away by one-side irardiation

8.4.4 Results

Three specimens are irradiated in the test stand. These are CF 2.0, CF 4.0 and CF ABS of the dimension d32. CF 2.0 and 4.0 pipes are tested according to the structure of Figure 58, while CF ABS is irradiated when installed and has a length of five meters.
The evaluation shows the temperature profile with maximum warpage and images from the thermal camera.

8.4.4.1 CF 2.0 d32/D75

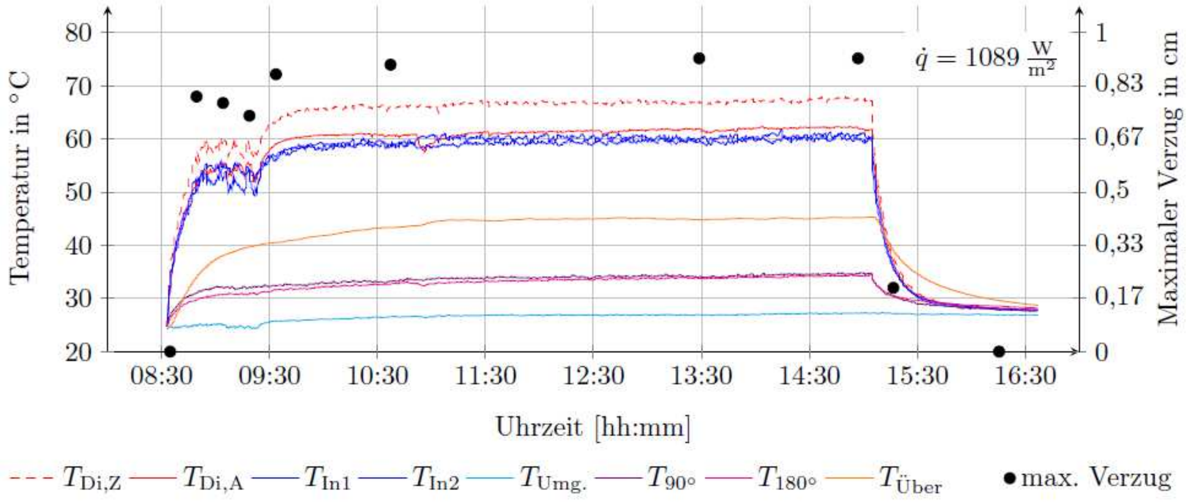

Figure 60: Temperature recording and maximum moving away for CF 2.0 d32/D75

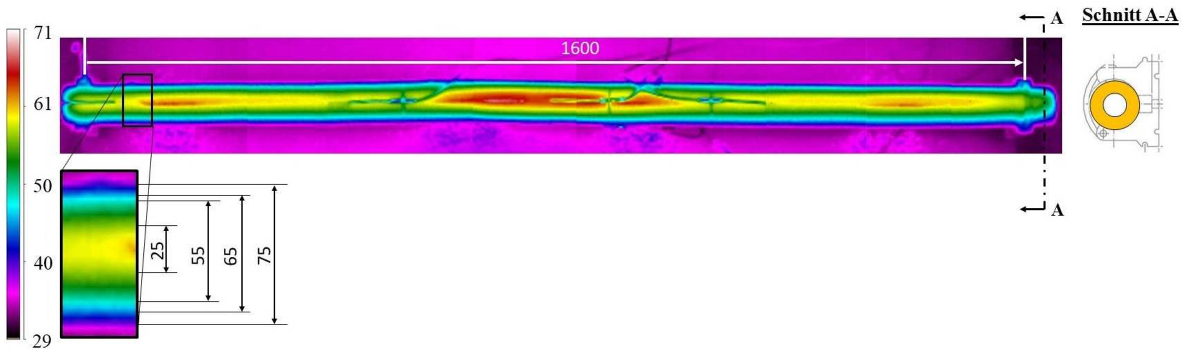

Figure 61: Image by the thermal camera for CF 2.0 d32/D75 at 14:30 from the top

By having a look at Figure 60, it is noticeable that the temperature in the directly irradiated area of the center is warmer. The reason is a temperature overlay of all three spotlights. The higher temperature is also evident in the thermal camera. When comparing this recording with the measured temperatures, there is agreement. At approximately 68 °C of the PT-element in the directly irradiated area shows he the same value as the legend of the thermal camera at the corresponding location. The same applies to all other temperature sensors. The settings of the irradiation to a constant surface temperature of about 60 °C are maintained and there is a balanced temperature over the entire length, as the recording of the thermal camera at 14:30 shows. In addition, at the beginning of the measurement between 08:30 and 09:30 o'clock a colder temperature than after 09:30 o'clock can be observed. This happens due to an open window, causing a draft to cool the surface. A maximum moving away is measured to approximately 0,95 cm throughout the experiment. As can be seen, the pipe reacts quickly to the different temperatures. After switching on and after switching off the spotlights, it returns quickly to its original form. The draft between 08:30 and 09:30 has the effect that the maximum moving away in this time is lower than after 09:30.

8.4.4.2 CF 4.0 d32/D90

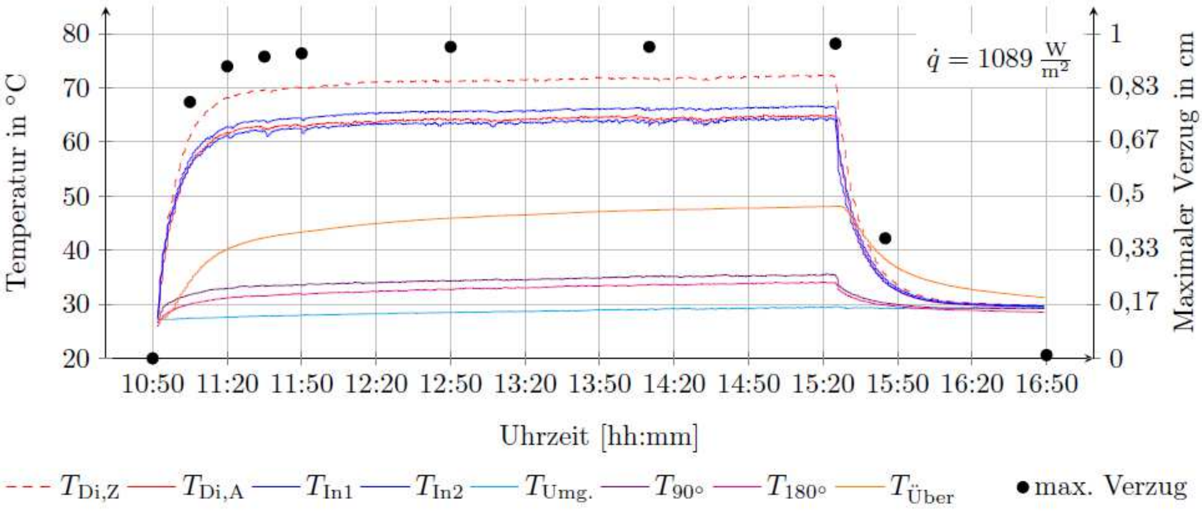

Figure 62: Temperature recording and maximum moving away for CF 4.0 d32/D90

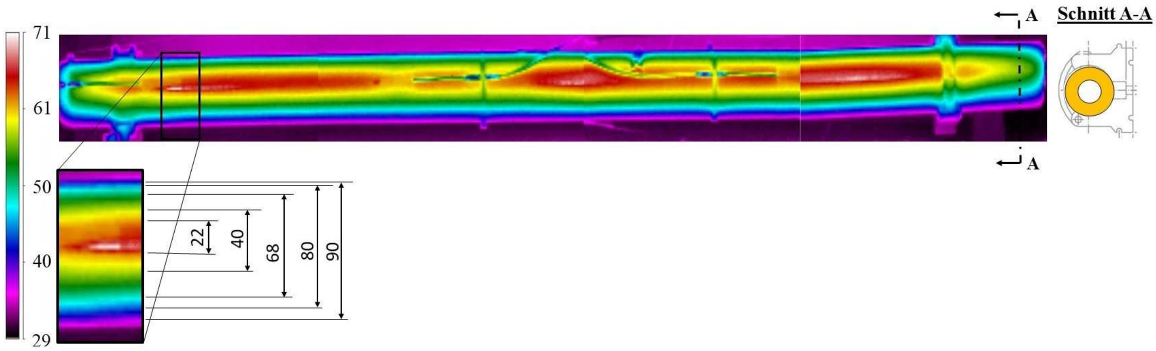

Figure 63: Images of the thermal camera for CF 4.0 d32/D90 at 15:20 from the top

The results of CF 2.0 are also evident in CF 4.0. The difference between the two measurements is the higher ambient temperature of about 5 K. This has an effect on the surface temperature, as observed in preliminary experiments that for CF 4.0 the average is about 65 °C. A constant surface temperature distribution is set, as the image of the thermal camera shows. The temperature of $T_{Di,Z}$ is higher, due to the temperature overlay of all the spotlights.

The effect on the maximum moving away is negligible, as for CF 2.0, about 0,95 cm. Equally, this specimen also returns to its original position during the cooling process, after the spotlights have been switched off.

The thermal camera shows also the temperature profile of the circumference. This results in a hot soul with an approximate width of 22 mm, when the pipe is irradiated from the top. The enlarged extract shows the approximate widths. The barely recognizable outer pink boundary layer therefore, has a temperature of approximately 34-40 °C, which is also measured by the temperature sensor $T_{90°}$. There is a little difference between $T_{90°}$ and $T_{180°}$.

8.4.4.3 CF ABS d32/D90

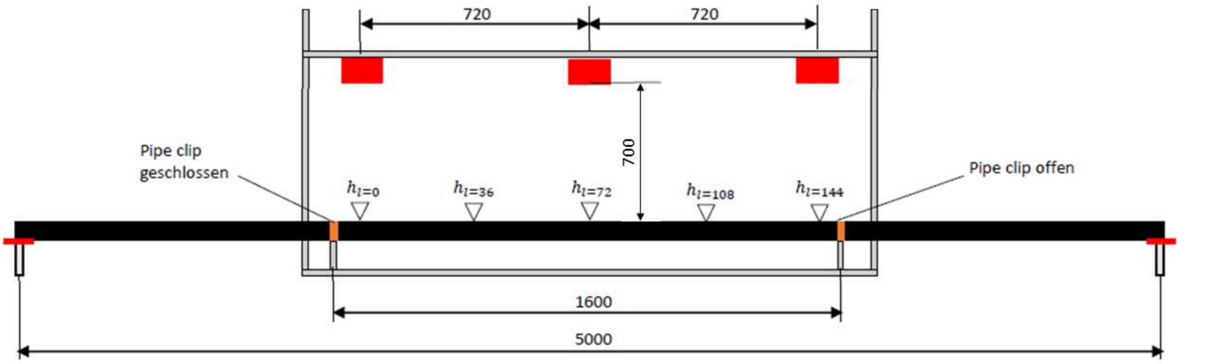

Figure 64: Test construction for the irradiation of CF ABS d32

The experimental design of CF ABS differs from that of CF 2.0 and CF 4.0. The test pipe has a length of five meters. As with CF 2.0 and CF 4.0, the area between the pipe clips is irradiated. The free ends are supported, so that the pipe is horizontally in the experimental setup. This test arrangement corresponds to the usual pipe holder in practice.

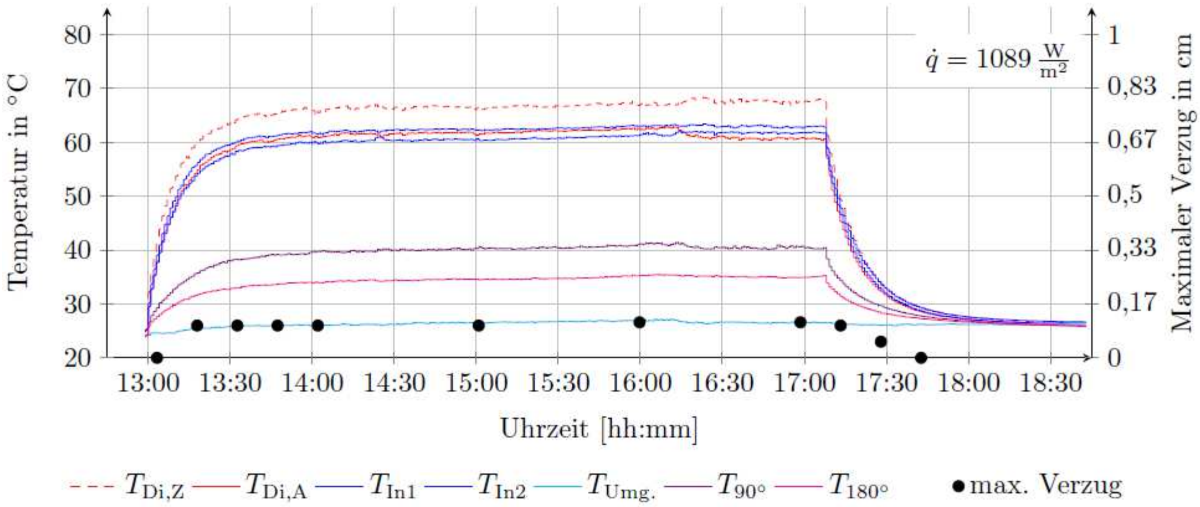

Figure 65: Temperature recording and maximum moving away for CF ABS d32/D90

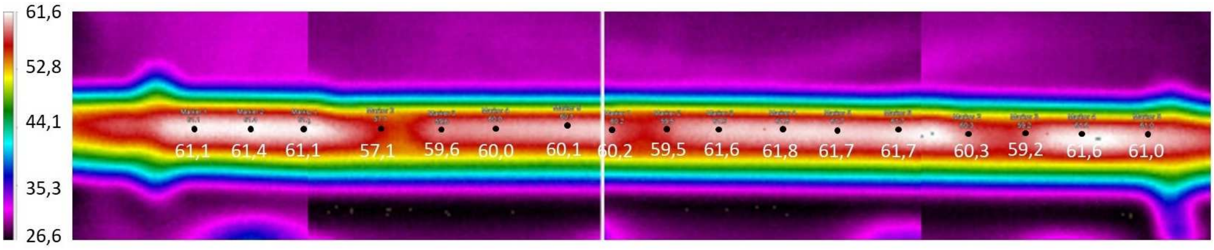

Figure 66: Image of the thermal camera for CF ABS d32 at 17:00 from the top

The results of CF ABS differ from CF 2.0 and 4.0. The pipe is held in the pipe clips and can´t warp due to the support of both free ends. With a maximum warpage of one millimeter, which is almost no longer measurable, the statement can be made that the pipe does not warp. The temperature profile is constant at about +60 °C. The directly irradiated sensor in the center measures a higher temperature due to the temperature overlap. This area is missing in the thermal camera.

Figure 67: CF ABS without irradiation

Figure 68: CF ABS irradiated

8.4.4.4 Evaluation

Only pipes that are stored in the nature and are not installed can warp due to the one-sided irradiation. At an irradiated length of 1,60 meters maximum warpage is about one centimeter. When cooled, the pipes return to their original position. Maximum warpage does not differ between CF 2.0 and CF 4.0 pipes.

A firm installation does not allow for warpage. This statement could be sustained on the specimen CF ABS where warpage was < one millimeter, so not really worth mentioning. For this reason, no further tests are being carried out at this point. Filled pipe will absorb the induced heat better resulting in an even lower no more apparent max. warpage.

Finally, it has to be said that additional factors are important in the nature. These are, for example, winds, shadows or the sun's position. Especially winds have an effect on the surface temperatures, as can be seen in the tests. Due to forced convection heat from the hot surface is released to the passing air.

9 Conclusion

As a final summary it can be said that this work examines extensively different stress situations of Georg Fischer pipes. These were initially, based on previous measurements, the force generation with axial clamping, as well as the L-Bend buildup. The results of both experiments partially coincided with those of the predecessor. In the axial force constraint, reference values for the force arising between -30 °C and +60 °C could be obtained. When compared to previous measurements, the results could be explained as plausible and showed a tendency. With slightly larger readings and an increasing difference to low temperatures, the results of the work met expectations. The L-Bend buildup showed great agreement between previous measurements and the results of this work for the thermally induced force generation. Only the excess deflection test showed no clear tendency and should be verified on occasion with further measurements.

In a further experiment, the thermal change in length of multilayer glass fiber pipes was investigated by temperature changing. Helpful results could be obtained. A clear trend shows the reliability of the measurement, so that expansion decreases with increasing glass fiber content.

The most detailed attempt was concerned with the time-dependent deflection behaviour. The results were of great importance, because there have been no measurements in this regard and no literature references to the investigated temperature ranges. The results showed clearly the behaviour of the investigated plastics, both in modulus of elasticity and in creep resistance. Across metrics, such as between CF ABS and single pipe ABS or CF 2.0 and 4.0 and PE-100, large matches could be found. Reproducibility tests showed a scatter of the results. With regard to the use of the results, these can be used in many ways. On the one hand, insights into the temperature behaviour of various plastics have been gained. Different applications presuppose that behaviour is known in this regard.

In the last experiment, the artificial irradiation of the pipes was examined by partial heating of the surface temperature on their dimensional stability. In this case, a warpage of the pipes could be found if they are irradiated on one side. When installed, however, no significant warpage can be measured. After cooling, all pipes returned almost completely back to their original shape. On the basis of these results, customers can be ensured that pipes do not warp in a way that installation is being negatively impacted. Nothing will happen once the piping system is installed permanently.

As an outlook, further work is in progress. It is intended to repeat and verify scattering measurements in order to increase the overall number of verified data points (statistics). In further experiments, the bursting behaviour, especially at lower temperatures will be investigated more in detail.

However the present and comprehensive findings have already been implemented into the GF theoretical calculation and simulation model. As a result GF is in the position to accurately predict the behaviour of any piping system and installation beforehand.